

AD 715438

TECHNICAL REPORT

THE FEASIBILITY AND USE OF ANTI-TORQUE SURFACES IMMersed IN HELICOPTER ROTOR DOWNWASH

by: C. Tung, J.C. Erickson, Jr. and F.A. DuWaldt

CAL No. BB-2584-S-2

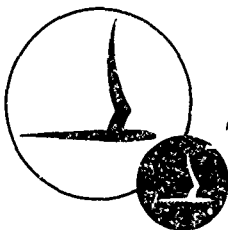
Prepared for:

Office of Naval Research
Aeronautics
Code 461
Arlington, Virginia 22217

Contract N00014-68-C-0241
NR 212-182
February 1970

Reproduction in whole or in part
is permitted for any purpose of
the United States Government.

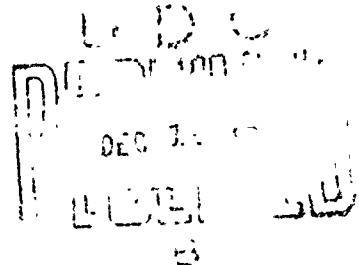
This document has been approved
for public release and sale; its
distribution is unlimited.



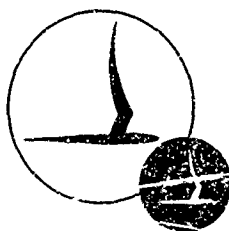
CORNELL AERONAUTICAL LABORATORY, INC.

OF CORNELL UNIVERSITY, BUFFALO, N. Y. 14221

Reproduced by
NATIONAL TECHNICAL
INFORMATION SERVICE
Springfield, Va. 22151



5/6



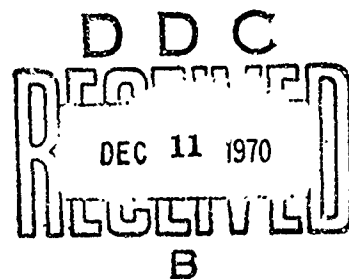
CORNELL AERONAUTICAL LABORATORY, INC.
BUFFALO, NEW YORK 14221

THE FEASIBILITY AND USE OF ANTI-TORQUE SURFACES
IMMERSED IN HELICOPTER ROTOR DOWNWASH

by

C. Tung, J.C. Erickson, Jr. and F.A. DuWaldt

CAL REPORT BB-2584-S-2
CONTRACT N00014-68-C-0241
NR 212-182
FEBRUARY 1970



Reproduction in whole or in part
is permitted for any purpose of
the United States Government

Prepared for:
OFFICE OF NAVAL RESEARCH
AERONAUTICS
CODE 461
ARLINGTON, VIRGINIA 22217

This document has been approved for public
release and sale; its distribution is unlimited.

SUMMARY

Losses of helicopter tail rotors occur with sufficient frequency to justify the search for a substitute system or, at least, an emergency device that would permit flight continuation (power on) and landing. CAL has shown previously that the use of aerodynamic surfaces immersed in the main rotor downwash to balance engine torque in the hovering flight mode is impractical in the sense that very large surface areas would be required. The current study is addressed to the problem of maintaining torque trim in the forward flight mode where the flight speed contributes to the dynamic pressure acting on the surface. It is shown that added surfaces giving total areas equal to about 2% of the main rotor disk area would provide torque trim for speeds above about 75 ft/sec for representative current vehicles. This capability should permit a roll-on powered landing in the event of tail-rotor failure.

The required surface size is not, itself, so great as to be impractical. Location and distribution of the surface area, however, is a problem if surfaces are to be retrofitted to many existing helicopters since the most effective location would probably be limited due to clearances between mechanical components. Therefore, incorporation of the tail boom as part of the tail area and introduction of active systems like jet flaps or movable surfaces to increase the achievable lift coefficient are considered. It is concluded that potential gains in safety margins, aural detectability, vibration and fatigue life of the tail rotor blades can be realized with carefully designed anti-torque augmenters. However, their use should be anticipated in the original design layout of the vehicle.

Recommendations are made for further design studies and experimental measurements.

TABLE OF CONTENTS

	<u>Page</u>
SUMMARY	ii
LIST OF ILLUSTRATIONS	iv
LIST OF SYMBOLS	vi
I. INTRODUCTION	1
II. TORQUE REQUIREMENTS	3
2.1 High Speed Flight Conditions - UH-1B	3
2.2 Generalization of High Speed Flight Conditions	6
2.3 Examples Based on Representative Helicopters	7
III. AERODYNAMIC CHARACTERISTICS OF ANTI-TORQUE SURFACES	10
3.1 Fixed Surfaces	10
3.2 Summary of Capabilities and Limitations of Fixed Surfaces	13
3.3 Movable Surfaces and High Lift Devices	14
IV. DISCUSSION AND CONCLUSIONS	19
V. RECOMMENDATIONS	22
VI. REFERENCES	23
APPENDIX A - POWER REQUIRED FOR A ROTOR	26
APPENDIX B - LIFT COEFFICIENT FOR FINNED ELLIPSE	28
APPENDIX C - FLAPPED FUSELAGE	30
DISTRIBUTION LIST	

LIST OF ILLUSTRATIONS

<u>Figure</u>		<u>Page</u>
1	Anti-Torque Moment Available from Aerodynamic Surfaces to Balance Main Rotor Torque - Bell UH-1B Helicopter, 6550 lb gross weight, 314 RPM	32
2	Flight Velocity for Minimum Power, V_{min} , as a Function of Sectional Drag Coefficient, $C_{d,o}$, Solidity, σ , Tip Speed, V_t , and Equivalent Flat Plate Area Ratio, f/A	33
3	Minimum Power, P_{min} , as a Function of Sectional Drag Coefficient, $C_{d,o}$, Solidity, σ , Tip Speed, V_t , and Equivalent Flat Plate Area Ratio, f/A	34
4	Anti-Torque Performance of a 2% Tail - Power, P_2 , as a Function of Flight Velocity for Minimum Power, V_{min} , and Tip Speed, V_t	35
5	Schematic Diagram of a UH-1C With Increased Tail Area	36
6	Possible OH-6A Modifications	37
7	Possible UH-2 Modifications	38
8	Possible SH-3D Modifications	39
9	Possible CH-53A Modifications	40
10	Possible UH-1C Modifications	41
11	(a) Effects of Aspect Ratio on Variation of Lift Coefficient With Angle of Attack. Rectangular Tips. 0° Yaw (Data from Reference 16)	42
	(b) Effects of Aspect Ratio on Variation of Lift Coefficient With Angle of Attack. Semicircular Tips. 0° Yaw (Data from Reference 16)	42
12	Aerodynamic Characteristics of NACA 66(215)-216 Airfoil Section With 0.20c Sealed Plain Flap (Reference 17)	43

<u>Figure</u>		<u>Page</u>
13	Theoretical and Experimental Part-Span Lift Factors for Two Models (Reference 18)	44
14	A Schematic Diagram of a UH-1A Profile with the More Important Dimensions Labeled	45
15	The Intersection of the Curves of F_1 and F_2 With $C_{d,p} = 0.013$, $f/A = 0.01$, and $\sigma (V_t/V_\infty)^2$ Varying Between 0.8 and 3.6	46
16	Flapped Fuselage of Elliptical Cross-Section in Transformed and Physical Plane	47
17	Flapped Fuselage of Circular Cross-Section in Transformed and Physical Plane	48

LIST OF SYMBOLS

A	main rotor disk area, ft. ²
A_b	rotor blade area, ft. ²
AR	aspect ratio
a	major axis of an ellipse, ft.
b	minor axis of an ellipse, ft.
C_L	lift coefficient
C_{LFR}	lift coefficient of finite span surface
C_{Lmax}	maximum lift coefficient
$C_{L\infty}$	lift coefficient of infinite span surface
$C_{L\alpha}$	$= dC_L/d\alpha$
C_T	thrust coefficient
$C_{d,0}$	sectional drag coefficient
F	part-span lift factor
F_t	anti-torque force, lbs.
f	flat plate area, ft. ²
K_1	ground clearance of fuselage-tail boom juncture, ft. (Figure 14)
K_2	ground clearance of tail skid, ft. (Figure 14)
K_3	hub height relative to tail boom, ft. (Figure 14)
k	$= \sqrt{\frac{a^2 - b^2}{4}}$, half distance from ellipse center to focus, ft.
l_t	distance between center of force and the rotor shaft axis, ft.
l_1	length of fin on the upper side of the fuselage, ft.
l_2	length of fin on the lower side of the fuselage, ft.

m_1	transformed length of l_1 , ft.
m_2	transformed length of l_2 , ft.
P	power, horsepower
P_{min}	minimum power required for flight, horsepower
P_2	power corresponding to torque that can be balanced by a vertical tail of area $0.02A$, horsepower
p	semi-perimeter/span
Q	main rotor torque, ft. lbs.
R	radius of the rotor blade, ft.
S_t	area of vertical tail, ft. ²
S_{t_0}	original area of vertical tail, ft. ²
T	thrust, lbs.
U	incoming flow velocity, ft./sec.
V	flight speed, ft./sec.
V_{min}	speed at which the power, P , required for flight is a minimum, ft./sec.
V_0	slipstream velocity, ft./sec.
V_t	tip velocity, ft./sec.
v	induced velocity, ft./sec.
W	weight of the aircraft, lbs.
α	angle of attack (related to the near wake twist parameter of Reference 1)
α_{STALL}	angle of attack at stall
δ	angle of the axis of vortex cores with respect to the freestream
Γ_0	circulation at mid-span, ft. ² /sec.
γ	yaw angle of incoming flow

μ	advance ratio
ρ	density of air, slugs/ft. ³
Ω	rotor rotational speed, rad./sec.
α	twist angle of Reference 1, ratio of swirl velocity to inflow velocity
σ	solidity, ratio of blade area to disk area

I. INTRODUCTION

Tail rotors on helicopters appear to be major factors in accidents and vehicle maintenance cost. Further, they are important noise and vibration sources. The objective of this investigation is the determination of the feasibility of using fixed aerodynamic surfaces immersed in the main rotor downwash to obtain helicopter anti-torque moments. It was determined in a prior study (Reference 1) that the replacement of the standard tail rotor on a helicopter by a fixed aerodynamic surface is not practical. The thesis of that study was that the high velocity slipstream regions underneath a rotor could provide sufficient dynamic pressure to permit the generation of relatively large lifts, and that these lifts could be vectored to provide anti-torque moments for the machine. The most stringent flight condition was inspected, namely, hovering within ground effect. Slipstream flow fields calculated previously (References 2-7) were used for the purpose of estimating aerodynamic forces, and it was found that the anti-torque function could be carried out by a suitably placed surface. This surface area appeared to be too large for operational application. On the other hand, in view of the rather conservative choice of lift coefficient, combined with the severe requirement of tail-rotor elimination, the calculations could not be considered as being all conclusive. That is, no close definition of the surface location and form had been made--and, hence, no limits on achievable forces had been designated--which would indicate the operating regime in which a practical surface would be effective. This has been done in the study reported here. The relationship between physical parameters of the vehicle, flight conditions, and specified tail size have been established under the postulate of small auxiliary surfaces on the helicopter fuselage for the purpose of augmenting the tail rotor.

The tail rotor is an efficient component in the hovering flight condition. In high speed flight, however, conventional aerodynamic surfaces become efficient force generators while the auxiliary disadvantages of tail rotors become more severe due to factors such as noise, vibration,

reliability and vulnerability. Consequently, there might be some advantage to providing a vertical tail that permits the unloading of the tail rotor and affords some anti-torque moment reserve in the event of loss of the tail rotor. Most current helicopters have at least a rough approximation to such a surface in the fairing normally built around the tail rotor support structure.

In the following sections the feasibility of using a relatively small conventional surface to provide anti-torque moments is established for the high speed flight condition--i. e., for flight velocities in excess of about 75 ft/sec. Both particular and generalized results are presented, and the possible shape of the surface is considered. It is noted that required surface size is not, itself, so great as to be impractical. Location and distribution of the surface area is, however, a problem if surfaces are to be retrofitted since the most effective location would probably be limited due to existing clearances between mechanical components.

No consideration was given to the effects of side gusts although this factor must be inspected eventually. Side gusts on the added surfaces can be expected to provide one of the control power conditions that must be met. Additionally, a lateral-longitudinal coupling might result due to the form of the pressure distribution on the tail and fuselage combination.

Incorporation of the tail boom as part of the tail area and introduction of circulation control to increase the achievable lift coefficient are considered. Direct power expenditure is implied for the jet-flap configuration. It is concluded that potential gains in safety margins, aural detectability, vibration and fatigue life of the tail rotor blades can be realized with carefully designed anti-torque augmenters. However, their use should be anticipated in the original design layout of the vehicle.

II. TORQUE REQUIREMENTS

It was found in Reference 1 that aerodynamic surfaces* with areas about thirty-five percent of the rotor disk area would be required for complete anti-torque balance of a typical vehicle hovering in ground effect. Since surfaces of this size are impractical, it was concluded that complete elimination of the tail rotor cannot be achieved in practice by conventional aerodynamic surfaces alone. There remains the question of the extent to which the tail rotor can be unloaded at flight conditions, other than lift-off and hover, through the use of aerodynamic surfaces that are a few percent of the rotor disk area in size.

2.1 High-Speed Flight Conditions - UH-1B

The present phase of the investigation was devoted to high-speed flight conditions, i. e., those in which the flight speed V of the helicopter is above the speed V_{min} at which the power P required for flight is a minimum, say P_{min} . Since we are concerned with torque balance, it is more useful to consider the power-required curves in terms of the main rotor torque Q which must be counteracted for moment equilibrium. The torque is related simply to the power required by the rotor rotational speed, namely, $P = Q\Omega$. For steady-state equilibrium, the anti-torque moment required is equal to Q , i. e.,

$$Q = F_t l_t \quad (1)$$

where

$$\begin{aligned} F_t &= \text{anti-torque force in lbs.} \\ l_t &= \text{distance between center of force} \\ &\quad \text{and the rotor shaft axis} \end{aligned}$$

*Operating at $C_L \approx 1$

If a tail surface is to furnish the anti-torque moment,

$$F_t = \frac{1}{2} \rho (V^2 + v^2) C_L S_t \quad (2)$$

where

$$\begin{aligned} \rho &= \text{density of air lb-sec}^2/\text{ft}^4 \\ V &= \text{helicopter forward speed, ft/sec} \\ v &= \text{induced velocity, ft/sec} \\ C_L &= \text{lift coefficient} \\ S_t &= \text{area of vertical tail, ft}^2 \end{aligned}$$

Equations (1) and (2) give

$$\begin{aligned} Q &= \frac{1}{2} \rho (V^2 + v^2) C_L \left(\frac{l_t}{R}\right) \left(\frac{S_t}{\pi R^2}\right) \pi R^3 \\ &= \frac{1}{2} \rho (V^2 + v^2) \frac{C_L l_t S_t}{RA} \pi R^3 \end{aligned} \quad (3)$$

where

$$\begin{aligned} A &= \pi R^2 = \text{main rotor disk area} \\ R &= \text{radius of the rotor blade} \end{aligned}$$

Calculations were made for a UH-1B to illustrate the above development. Rotor torque required (based on the power-required curve given in Reference 8) as a function of forward speed for the Bell UH-1B is given in Figure 1. The anti-torque moment available from aerodynamic surfaces completely immersed in the rotor downwash is also plotted in Figure 1 for three values of the nondimensional parameter $\frac{C_L l_t S_t}{RA}$.

For a given value of $\frac{C_L l_t S_t}{RA}$, the aerodynamic surface will exactly balance the rotor torque for that value of V where the corresponding curve intersects the anti-torque-moment-required curve. Above that V , the C_L would be reduced to provide trim for a given l_t and S_t and a force margin would be available for maneuvers. For $\frac{l_t}{R} = 1.213$ (which

corresponds to the position of the UH-1B tail rotor axis) and $C_L = 1.0$, an $\frac{S_f}{A}$ of 0.02 (i. e., two percent of rotor disk area) would balance the torque for all flight speeds above 75 ft/sec. This velocity is very close to V_{min} . The present UH-1B vertical tail has a value of $\frac{S_f}{A} = 0.0073$ ($\frac{C_L l_t S_f}{RA} = 0.00885$ for $C_L = 1$ on Figure 1) which just manages to balance the entire rotor torque near its maximum speed. Thus, for a threefold increase in tail area, the speed at which the torque is completely balanced will be reduced from the maximum speed of the helicopter to V_{min} . Redesign of the geometry of the tail might provide a C_L greater than 1.0 and, hence, permit use of a smaller area. Therefore, the tail rotor can be unloaded completely at speeds above 75 ft/sec, so far as anti-torque balance is concerned, by a reasonably sized vertical tail surface. Moreover, in the event of complete loss of the tail rotor at speeds above 75 ft/sec, as can occur for many reasons including foreign-object damage (Reference 9), such a tail surface would permit fully powered flight to speeds as low as 75 ft/sec. This speed is approximately the maximum speed for which a UH-1B can land on smooth ground without structural failure of the landing gear, as indicated by the height-velocity (H-V) diagram for this vehicle (Reference 10). Furthermore, this powered-flight capability should provide the pilot with sufficient flexibility for entering autorotation to permit landing at even lower speeds because of the practically negligible torque that must be balanced in the autorotational flight condition.

Results presented above establish the feasibility of increasing tail surface size for a particular configuration. Generalization of the analysis is presented in Section 2.2. In particular, V_{min} and P_{min} have been determined for general helicopter configurations based on a relatively simple power-required equation. As an example, the entire power-required curve has been worked out for the UH-1B and is presented as anti-torque moment required in Figure 1. The predicted Q_{min} is in excellent agreement with the flight-test value, although the corresponding predicted V_{min} is considerably higher than the test value. However, the torque-required curves are relatively flat around Q_{min} . Therefore, the error in the velocity at which a tail surface

would become effective is not large.

2.2 Generalization of High-Speed Flight Conditions

The feasibility of increasing tail surface size for a particular configuration was established in the previous section. This type of information may be generalized. In particular, V_{min} and P_{min} have been determined for a general helicopter configurations based on a relatively simple power-required equation (Reference 11). It is shown in Appendix A that the governing parameters for the power required are W , V_o , $C_{d,o}$, V_t , σ and f/A where W is the weight of the craft; V_o is the momentum-averaged value of the main rotor induced velocity in hover; $C_{d,o}$ is the mean rotor blade sectional profile drag coefficient; V_t is the rotor tip speed; σ is the solidity and f/A is the ratio of the fuselage equivalent-flat-plate-area to the rotor disk area. Computations of V_{min} and P_{min} have been made for a broad range of parameters that are typical of existing and presently envisioned helicopters. For example, $C_{d,o} = 0.013$ (Reference 12, Figure 5); $\sigma = 0.05$ to 0.12 ; $V_t/V_o = 16$ to 30 ; and $f/A = 0.0060$ to 0.014 (Reference 13, Figure 1). A useful working chart can be obtained by using these parameters. For example, Figure 2 shows V_{min}/V_o versus $\sigma (V_t/V_o)$ with f/A as a parameter. Given f , σ , W , V_t and A , we can calculate $\sigma (V_t/V_o)$. Then V_{min}/V_o can be read directly from Figure 2 for given f/A . For this V_{min}/V_o , Figure 3 shows the corresponding P_{min}/WV_o . Several examples will be given in the next section to illustrate the use of these curves.

If C_L is assumed to be one,* Equation (3) may be written, through the relation $P = Q \Omega$ and $v^2 = -\frac{V_t^2}{2} + \frac{1}{2} \sqrt{V_t^4 + 4V_o^4}$, as

$$\frac{l_t S_t}{RA} = \frac{\frac{\partial P}{WV_o}}{\frac{V_t}{V_o} \left[\frac{V_t^2}{V_o^2} + \sqrt{\left(\frac{V_t}{V_o}\right)^4 + 4} \right]} \quad (4)$$

* It should be noted that in order to derive Equation (4), the lift coefficient is assumed to be one. Methods for achieving or even possibly exceeding this value are discussed in Section 3.3 (Movable Control Surfaces and High Lift Devices)

Although the area ratio S_t/A is used in the previous section, it may be more convenient to use tail volume, $T_v = \ell_t S_t$, as a more appropriate parameter to represent any given anti-torque surface. T_v is limited to two percent of rotor disk area times the rotor radius and substituting V_{min}/V_o (from Appendix A) in this equation, one obtains

$$\frac{P_2}{WV_o} = \frac{0.01 \frac{V_t}{V_o} \left(\frac{V_{min}^2}{V_o^2} + \sqrt{\frac{V_{min}^4}{V_o^4} + 4} \right)}{4}$$

where P_2 is called the upper bound power required to be balanced by the tail volume at two percent of RA . Figure 4 shows P_2/WV_o against V_{min}/V_o with V_t/V_o as a parameter. This figure may serve as a guide as to whether or not the P_{min}/WV_o for a typical helicopter flying at V_{min}/V_o can be balanced by two percent of RA . It will show in the next section that several existing helicopters do indeed meet this requirement.

2.3 Some Examples Based on Representative Helicopters

The Hughes OH-6A, the Kaman UH-2C, the Sikorsky SH-3D and the Sikorsky CH-53A are used as examples (the Bell UH-1B was treated in the previous section). The following table shows the physical parameters and estimated aerodynamic parameters for these vehicles.

ITEM	VEHICLE			
	OH-6A	UH-2C	SH-3D	CH-53A
WEIGHT, W, LBS.	2400	9600	18600	33000
DISC AREA, A, FT ²	544	1520	3020	4070
NO. OF BLADES, N _b	4	4	5	6
SOLIDITY, σ	0.054	0.104	0.073	0.115
FUSELAGE FLAT PLATE AREA, f, FT ²	7	13	31	44
TIP SPEED, V _t , FT/SEC	646	640	700	700
BLADE PROFILE DRAG COEFFICIENT, C _{d,o}	0.013	0.013	0.013	0.013

In order to calculate the V_0 , the density $\rho = 0.00234$ slugs/ft³ is used for all the computations. According to the formulas in Section 2, the parameters such as V_0 , V_t/V_0 , f/A and $\sigma V_t/V_0$ are computed to be the following:

ITEM	VEHICLE			
	OH-6A	UH-2C	SH-3D	CH-53A
V_0 , (ft/sec)	30.7	36.7	36.2	41.6
V_t/V_0	21.0	17.5	19.3	16.8
f/A	0.0130	0.0085	0.0100	0.0110
$\sigma V_t/V_0$	1.13	1.82	1.41	1.94

By using the above tabulated numbers, we find V_{min}/V_0 , P_{min}/WV_0 and P_2/WV_0 from Figures 2, 3 and 4 and convert to:

ITEM	VEHICLE			
	OH-6A	UH-2C	SH-3D	CH-53A
V_{min} (ft/sec)	95	122	118	131
P_{min} (hp)	120	590	1100	2350
P_2 (hp)	140	630	1270	2100
{ TORQUE PROVIDED BY 2% TAIL } { TORQUE TO BE BALANCED } { AT SPEED FOR MINIMUM POWER }	1.2	1.1	1.2	0.9

The above tabulation indicates that V_{min} is probably above the landing speed permitted by the landing gear design.

The important conclusion is that the helicopter may be landed at lower speeds than V_{min} while the torque to be balanced is still within the limitation of a tail volume achievable with a two percent tail area ratio. The exception is the CH-53A.

It seems, at the present stage, that there are two ways to modify the performance of the current helicopter. First, the tail surface may be redesigned or modified and, second the landing gear might be redesigned

to permit landing at higher speeds. However, it should be kept in mind that the above conclusion is based on the assumption that the lift coefficient of the tail surface is equal to unity. Hence, the aerodynamic characteristics of the tail surface and possible high lift devices will be discussed in the next two sections.

III. AERODYNAMIC CHARACTERISTICS OF ANTI-TORQUE SURFACES

3.1 Fixed Surfaces

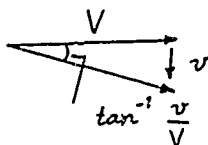
It has been shown in previous sections that two percent of rotor disk area may be sufficient to balance engine torque if the moment arm has a length of one blade radius. The placement of the anti-torque surface presents a difficult problem for existing helicopters, however, due to constraints imposed by current geometrical configurations. However, we shall discuss a general approach to the problem, and indicate specific application to representative helicopters such as the OH-6A, UH-2C, SH-3D and CH-53A.

For current helicopters, the size of the tail surface is less than two percent of the rotor disk area. The simplest and most direct method of achieving the desired area is to increase the existing tail surface to the required size. The tail surface should be designed in such a way that the lift coefficient of the tail surface could be equal to one without the requirement for large fuselage yaw angles in order to achieve the required effective angle of attack. On the other hand, it may not be practical to increase the size of the tail surface and, hence, the anti-torque surface could be mounted on the body as for example, in Figure 5. This figure illustrates a schematic diagram of a modified UH-1C wherein the cross-hatching indicates added areas that would be effective for torque compensation. The sections at A-A and B-B are also shown.

Possible anti-torque surfaces are also given for OH-6A, UH-2C, SH-3D, CH-53A and UH-1C in Figures 6, 7, 8, 9 and 10. In each figure the top sketch is the unmodified vehicle, the middle sketch represents a possible fuselage flap configuration whereas the lower sketch represents an enhancement of the existing vertical tail. In each case an attempt was made to retain the configuration within limitations imposed by clearance requirements. Attainment of a two percent tail surface appears to be feasible in some cases if the fuselage area above the flap is effective.

The flow direction, which depends on the flight and induced velocities may be computed as follows:

$$\frac{v}{\Omega R} = \frac{C_T}{2 \left[\left(\frac{V}{\Omega R} \right)^2 + \mu^2 \right]^{1/2}}$$



where

$$C_T = \text{thrust coefficient} = \frac{T}{\pi R^2 \rho (\Omega R)^2}$$

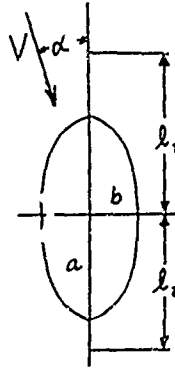
$$\mu = \text{advance ratio}$$

We shall consider the UH-1B as an example, and for a representative $C_T = 352 \times 10^{-4}$ obtain the following flow directions.

V, ft/sec	v, ft/sec	$\tan^{-1}(v/V)$, deg
16.7	27.8	59
33.3	22.3	33.8
50.0	16.9	18.6
66.7	13.2	11.2
83.5	10.7	7.3
100.0	9.0	5.1
117.0	7.7	3.8

It is apparent that the flow direction changes markedly with flight speed. At low flight speed, the combination of tail surface, body and added surface is representative of a wing with high aspect ratio while at high flight speed, the configuration is more representative of a low aspect ratio wing. Consequently, the value of the lift curve slope changes with flight speed as equivalent aspect ratio changes. It is difficult to calculate exact lift coefficient for such unusual shapes but values may be estimated for the limiting cases of high or low aspect-ratios.

At low flight speed, the aspect-ratio is high and the flow over an anti-torque surface can be represented in the following manner.



The angle α is related to the near-wake twist parameter \mathcal{X} (Reference 1) where \mathcal{X} is the ratio of the tangential component to the axial component of the slipstream velocity. The body may be represented by an elliptical or circular cylinder, and the lift coefficient of this configuration can be computed if we assume the flow to be inviscid and incompressible. Details of the computation are given in Appendix B. The lift coefficient is found to be:

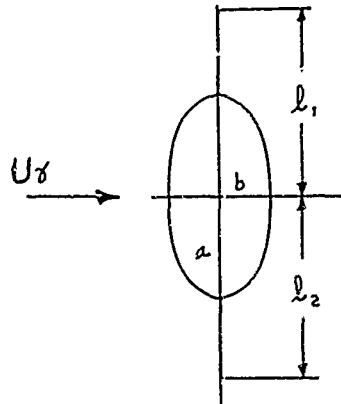
$$C_L = 2\pi\alpha \left\{ 1 + \frac{b}{2a} \left[\frac{1 + b/a}{\frac{m_1 m_2}{a^2} \left(\frac{m_1 m_2}{a^2} + \frac{1 - b^2/a^2}{4} \right)} \right] \right\}$$

where

$$\frac{l_1}{a} = \frac{m_1}{a} + \frac{k^2/a^2}{m_1/a}, \quad \frac{l_2}{a} = \frac{m_2}{a} + \frac{k^2/a^2}{m_2/a} \quad \text{and} \quad \frac{k^2}{a^2} = \frac{1 - (b^2/a^2)}{4}$$

Consider the following example. Let $b/a = 1.0$, $\frac{l_1}{a} = \frac{l_2}{a} = 2$ then $C_L = 2\pi\alpha \left[1 + \frac{1/2^2}{2^2} \right] = 2\pi\alpha \left(1 + \frac{1}{16} \right) = 2\pi\alpha (1.0625)$. However, when $a = b$, the central body is a circular cylinder and the flow over such a body will separate if viscous effects are considered. Hence, it is questionable whether this lift coefficient can be achieved in practice.

At relatively high flight speed, the aspect ratio is reduced and the so-called Jones theory for low aspect ratio wings may be applied. The following sketch illustrates the problem



where γ indicates the yaw angle of the incoming flow. The same type of analysis as that in Appendix B gives the following lift coefficient:

$$C_L = \frac{\pi}{2} \gamma AR \left[1 + \frac{b}{2a} \frac{\left(1 + \frac{b}{a}\right)}{\frac{m_1 m_2}{a^2} \left(\frac{m_1 m_2}{a^2} + \frac{1 - \frac{b^2}{a^2}}{4}\right)} \right]$$

where AR is usually less than one.

For this case it can be shown that it is difficult to achieve high lift coefficients for the small values of γ that are required in order for this theory to be valid. Fortunately, the nonlinear effects on lift are favorable.

3.2 Summary of Capabilities and Limitations of Fixed Surfaces

The fixed vertical tail of modest size can provide trim torque balance at all speeds above the speed for minimum power required. However, the flow direction over the surface (vector sum of main rotor downwash and forward flight velocity) changes continuously with flight speed. Both angle of attack and effective aspect ratio change are affected. It might be possible

to choose that combination of surface twist and area distribution that would provide nearly constant (zero) yaw angle over the flight range.

Effectiveness of the schemes which depend on generation of circulatory forces on tail boom shell (middle sketches) are open to question. It is presumed that the effective area encompasses the fuselage area above and below the added plate-like surfaces. Thick airfoil data generated by propeller manufacturers afford some justification for believing maximum lift coefficients of the order of unity can be attained if the camber line is carefully chosen.

The requirement for a maneuvering capability naturally raises the question of the feasibility of providing a movable control surface element or some other means for modulating and incrementing the force generated. Such active devices are considered in the next section.

3.3 Movable Control Surfaces and High Lift Devices

The discussions of tail areas required in the previous sections are based on the assumption that the maximum lift coefficient is to be at least unity. The immediate question is how to achieve this value easily for the unusual shapes discussed before. In order to answer this question, it is necessary to inspect the limiting lift coefficient of a conventional airfoil with finite aspect ratio.

The effective aspect ratio of the counter torque surface changes with flight speed because the direction of the resultant velocity at the surface changes. For the untapered wing, an empirical formula which reproduces the theoretical curve for the rectangular wing down to aspect ratios close to one is given by (Reference 15)

$$C_{L\alpha} \approx \frac{2\pi AR}{\rho AR + 2} \quad (5)$$

where

$$p = \frac{\text{semi-perimeter}}{\text{span}}$$

This formula also holds for arbitrary sweep.

In case of zero sweep $p = \frac{AR + 1}{AR}$
then

$$C_{L\alpha} \approx \frac{2\pi AR}{AR + 3} \quad (6)$$

The maximum lift coefficient for a wing depends on both the aspect ratio and the angle at which stalling occurs:

$$C_{L_{max}} \approx \frac{2\pi AR}{p AR + 2} \alpha_{STALL} \quad (7)$$

As the aspect ratio decreases, the lift-curve slope also decreases, but the angle of attack at which stall occurs increases. In fact, the results of systematic tests indicate $C_{L_{max}}$ is roughly constant. For example, C_L data obtained from tests with systematic variations of aspect ratio (Reference 16) are shown in Figure 11. It is clear from Figure 11 that a maximum lift coefficient greater than 1.0 can be achieved if the corresponding angle-of-attack distribution can be imposed. The nonuniformity of the velocities in the rotor wake suggests that attainment of a net C_L of 1.0 in the operating range of interest would require a variable geometry (mechanical flap or rudder) or a lift augmentor (jet flap). Such active systems have the obvious advantage of providing variable forces for trimming and maneuvering.

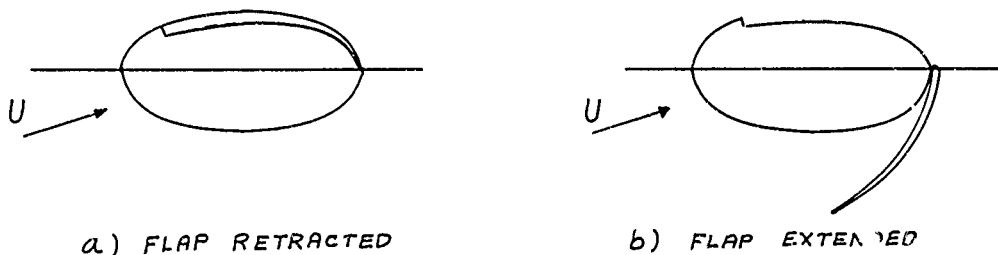
Mechanical flaps have been investigated extensively in the past several decades. The work by Abbott and Von Doenhoff (Reference 17), for example, gives an excellent survey. The aerodynamic characteristics

of a special airfoil section [NACA 66 (215)-216] with a 20 percent chord flap are shown in Figure 12 from Reference 17. It indicates that section lift coefficients of unity may be obtained at zero angle of attack with high deflection angle of the flap. The finite-aspect-ratio effect on a mechanical flap has been discussed by Foster (Reference 18). The equation is similar to Equation (5) for the unswept wing, except for a correction factor applied to the lift coefficient, i. e.,

$$C_{L_{AR}} \approx \frac{AR C_{L_{\infty}}}{AR + 3} (F) \quad (8)$$

where F is called the part-span lift factor and is a function of the ratio of the span of the flap to the span of the wing. Theoretical and experimental part-span lift factors for two models are shown in Figure 13 reproduced from Reference 18. The curve for F may be approximated by a straight line. For $F = 1.0$ and $(C_{L_{\infty}})_{max} = 2.0$ (this value is given by using split flaps at 60 degrees, Figure 2, Reference 19), the aspect ratio has to be three in order to achieve $C_{L_{AR+3}} = 1.0$.

The concept of mechanical flap may also be applied to the body with elliptic or circular cross section as shown on the following schematic diagram:



The calculation of the lift coefficient is given in Appendix B. It shows that higher lift coefficient (say, 2.0) may be generated. But, when the effect of finite aspect-ratio is considered, the lift coefficient of value one might not be achieved.

The jet flap, on the other hand, will produce not only the lift due to effective camber but also the reaction lift. Therefore, this device can be effective even in the very low speed regime. Helmholtz (Reference 20) has shown that if the trailing vortex sheet has rolled up into a pair of concentric vortices and the momentum and the kinetic energy per unit length of the vortex system are conserved, then

$$C_L = \frac{\pi^3 AR}{4} \sin \delta \left[1 - \frac{\pi^2}{4} \sin^2 \delta \right] \quad (9)$$

where δ is the angle of the axes of the vortex cores with respect to the free stream and equal to $\sin^{-1} \frac{2 \Gamma_0}{\pi^2 b U}$ with Γ_0 = mid-span strength for the circulation, b = half span, U = free-stream velocity. C_L in Equation (9) has maximum value

$$C_{L_{max}} = \frac{\pi^3 AR}{3\sqrt{3}} = 1.9 AR \quad (10)$$

at

$$\delta = \sin^{-1} \frac{2}{\pi\sqrt{3}}$$

The highest value of C_L observed by Lockwood, Turner, and Riebe (Reference 21) in their jet-flap investigation is roughly twice the value of the aspect ratio of the wing tested, which confirms Equation (9). Recently, Erickson and Kaskel (Reference 22) have investigated the low-aspect ratio rectangular jet-flap control surfaces. Complete tables and curves of the computed lift and pitching-moment coefficients for different

configurations are presented over a wide range of aspect ratio and jet-momentum coefficients. It shows that $C_L = 1.0$ is easily achieved by using a jet flap.

The successful application of mechanical flaps and jet flaps to provide anti-torque moments for helicopters is complicated for the following reasons:

1. The shape of the aerodynamic surface is compromised by auxiliary conditions on clearances (see Section IV following).
2. The imposed flow field (i. e., the rotor wake and the wake-induced effects) varies continuously with speed.
3. The surface would probably be unsymmetrical with respect to the flow direction.
4. Interference effects introduced by the tail rotor, fuselage and tail boom may be significant.
5. Ground effect will be important for some flight modes.

IV. DISCUSSION AND CONCLUSIONS

The preceding analyses and calculations indicate that it is possible to generate substantial anti-torque moments with relatively small aerodynamic surfaces whose areas are approximately twice the size of those currently built around tail rotor support structures. In particular, it was found that the tail rotor on a helicopter could be unloaded when the forward speed is in excess of about 75 ft/sec. This feature could represent a substantial safety margin in the event of a tail rotor failure since the vehicle could be trimmed in yaw with power on at all speeds above 75 ft/sec. Thus, it would make possible power-on, roll-on landings provided the collapse limits of the landing gear were not exceeded.

It would be difficult, however, to extend the flight envelope to lower speeds wherein trim could be maintained without a tail rotor. Below the speed for which minimum power is required, the force (and, hence, the torque) that can be generated on the aerodynamic surface is decreasing since the dynamic pressure is decreasing. Simultaneously, the torque to be balanced is increasing. Very high lift coefficients, very large surfaces, or jet controls are indicated if the surface is fixed (Reference 1). The most critical requirement for the anti-torque may be the yaw acceleration specification in the slow rearward flight mode. Here, the torque reaction requirement is large and that portion of the surface which has the largest moment arm becomes ineffective because the slipstream no longer passes over it. As a result, the use of fixed surfaces for generating anti-torque forces must be augmented by some type of active system.

As denoted here, active systems such as movable mechanical flaps, boundary-layer suction, or jet flaps are means for obtaining high lift coefficients and provide convenient means for introducing control. Use of such systems would, hopefully, allow the generation of substantial side forces by incorporating a part of the tail boom as an active surface. But even these devices probably cannot compete with the tail rotor in hovering

in terms of thrust-to-power ratio. Any assessment of relative effectiveness and cost of an anti-torque system must be based on mission profile since the tail rotor is more effective in hovering while its substitute could be more effective in cruise.

Incorporation of a fixed vertical surface to alleviate tail rotor problems should be done at the preliminary design stage because retrofitting may become impractical. Limitations imposed by clearances are the most important, and these can be illustrated with a UH-1A profile and a few rules relating to configuration parameters. Figure 14 is a sketch of the UH-1A layout with the more important dimensions labeled. In the lower part of the figure are indicated the areas in which vertical surfaces are prohibited. In particular, to prevent strikes on the tail boom by the main rotor, the following approximate requirement is imposed:

$$K_3 > R/5$$

Rotation of the fuselage during a flare landing introduces the following condition:

$$K_1 + K_5 > R/5$$

Areas denied for placement of vertical tail surfaces are denoted by cross-hatched areas on Figure 14. A resulting possible configuration for increasing the area of the existing tail is shown. Note that only a small fixed surface could be placed on the underside of the boom and that the most effective part of the top side of the boom is not available because of possible mechanical interference with the main rotor.

In the previous discussion no consideration was given to possible degradation of tail rotor performance due to additional interference when the vertical fin size is increased. There are compensating effects. It appears that the loss in performance due to the imposed nonuniformity of the flow field is compensated by a favorable interference between the tail

rotor and the fin--that is, a part of the nonuniformity is a favorable change in the mean inflow to the tail rotor. There are other considerations relative to vertical tail and tail rotor matching, however. One of these is the modification of the generalized shaking forces applied to the tail rotor blades.

In part of the flight range, the tail rotor operates in the wake of the main rotor and experiences a pulsating inflow (References 23 and 24). It is highly desirable to avoid coincidence of tail rotor blade structural natural frequencies with the dominant forcing frequencies. Similarly, the nonuniform inflow imposed by the vertical tail should not produce an angle-of-attack variation on the tail rotor blades that will lead to large generalized forces at resonance frequencies. Therefore, minimization of the excitation of the tail rotor structural modes probably is the important design problem in matching the vertical tail size and location relative to the tail rotor.

V. RECOMMENDATIONS

Results of this investigation suggest the following recommendations:

- * Seek experimental verification of the conclusion that a vertical tail area that is two percent of the main rotor disk area will furnish a torque balance at flight speeds in excess of 75 ft/sec.
- * Inspect tail rotor design implications when a two percent tail surface is included in a configuration.
- * Conduct an experimental study of the maximum lift coefficient achievable with cylinders having flaps and/or slats.
- * Investigate the feasibility of using jet flaps on helicopter fuselages and/or vertical tails to achieve anti-torque moments over the complete flight spectrum.
- * Conduct a feasibility study of using an externally blown flap operating off the main engine exhaust for generation of anti-torque moments.

VI. REFERENCES

1. Sowyrda, A. On the Feasibility of Replacing a Helicopter Tail Rotor
Cornell Aeronautical Laboratory Report No. BB-2584-S-1 July 1968
(AD 677642).
2. Sowyrda, A. and DuWaldt, F. Representation of Wakes of Propellers in Ground Effect by Ring Vortex Systems Cornell Aeronautical Laboratory Interim Report BB-1665-S-1 April 1963.
3. Brady, W. G. and Crimi, P. Representation of Propeller Wakes by Systems of Finite Core Vortices Cornell Aeronautical Laboratory Summary Report BB-1665-S-2 February 1965 (AD 612007).
4. DuWaldt, F. A. Wakes of Lifting Propellers (Rotors) in Ground Effect Cornell Aeronautical Laboratory Final Report BB-1665-S-3 November 1966 (AD 643159).
5. Crimi, P. Theoretical Prediction of the Flow in the Wake of a Helicopter Rotor Part 1 - Development of Theory and Results of Computations Cornell Aeronautical Laboratory Final Report BB-1994-S-1 Part 1 September 1965 (AD 629782).
6. Crimi, P. Theoretical Prediction of the Flow in the Wake of a Helicopter Rotor Part 2 - Formulation and Application of the Rotor-Wake-Flow Computer Program Cornell Aeronautical Laboratory Final Report BB-1994-S-2 Part 2 September 1965 (AD629783).
7. Crimi, P. and Trenka, A. R. Theoretical Prediction of the Flow in the Wake of a Helicopter Rotor, Addendum - Effects Due to a Fuselage in a Constant, Nonuniform Flow Cornell Aeronautical Laboratory Report BB-1994-S-3 August 1966 (AD 637872).

8. Blankenship, B. L. and Harvey, K. W. "A Digital Analysis for Helicopter Performance and Rotor Blade Bending Moments" J. A. H. S. Vol. 7 No. 4 October 1962 pp. 55-68.
9. Kertoot, Jr., Lt. Col. Lester R. "Airframe FOD" U. S. Army Aviation Digest Vol. 15, No 5 May 1969 pp. 54-56.
10. Green, Lt. D. L. Helicopter Stability and Control as Related to Sudden Engine Failures-Autorotative Flight and Autorotative Landings Naval Air Test Center USNTPS-SP-No. 102, 7 November 1967.
11. Young, R. A. Helicopter Engineering Ronald Press Company 1949.
12. McCloud III, J. L., Biggers, J. C. and Maki, R. L. Full-Scale Wind-Tunnel Tests of a Medium-Weight Utility Helicopter at Forward Speeds NASA TN D-1887 May 1963.
13. Harris, F. D. "An Analytical Study of Rotor Performance at High Forward Speeds" Proceedings of the Seventeenth AHS Annual National Forum May 1961.
14. Gessow, A. and Myers, Jr., G. C. Aerodynamics of the Helicopter Frederick Ungar Publishing Company New York 1967.
15. Jones, R. T. and Cohen, D. "Aerodynamics of Wings at High Speeds" Princeton Series Vol. II Aerodynamic Components of Aircraft at High Speeds Editors: Donovan, A. F. and Lawrence, H. R. Princeton University Press 1957.
16. Zimmerman, C. H. Characteristics of Clark Y Airfoils of Small Aspect Ratios NACA Report 431, 1932.

17. Abbott, I. H. and Von Doenhoff, A. E. Theory of Wing Sections
Dover Publications, Inc. New York 1958.

18. Foster, D. N. "Some Aspects of the RAE High-Lift Research
Programme" The Aeronautical Journal of the Royal Aeronautical
Society Vol. 73 June 1969 p. 541 - 546.

19. McRae, D. M. "The Aerodynamics of High-Lift Devices on
Conventional Aircraft" The Aeronautical Journal of the Royal
Aeronautical Society Vol. 73 June 1969 p. 535 - 541.

20. Helmbold, H. B. "Limitations of Circulation Lift" JAS Vol. 24
March 1957 pp. 237 - 238.

21. Lockwood, V. E., Turner, T. R., and Riebe, J. M. Wind Tunnel
Investigation of Jet-Augmented Flaps on a Rectangular Wing to High
Momentum Coefficients NACA TN 3865 December 1956.

22. Erickson, J. C. and Kaskel, A. L. Theoretical Solutions and
Numerical Results for Low-Aspect-Ratio Rectangular Jet-Flap
Control Surfaces Therm Advanced Research, Inc. TAR-TR 6603
December 1966.

23. Robinson, F., Batra, N. N., Duhon, J. M. and Lynn, R. R.
"Tail Rotor Design Part I - Aerodynamics" AHS 25th Annual
National Forum Proceedings May 1969.

24. Balke, R. W., Bennett, R. L., Gaffey, T. M., and Lynn, R. R.
"Tail Rotor Design Part 2 - Structural Dynamics" AHS 25th Annual
National Forum Proceedings May 1969.

25. Glauert, H. Theoretical Relationships for an Aerofoil with Hinged
Flap British ARC, R & M No. 1095 1927.

APPENDIX A

Power Required For a Rotor

A relatively simple power-required equation for a general helicopter configuration is given in Reference 11 as

$$\begin{aligned}
 P_{\text{required}} &= P_{\text{induced}} + P_{\text{profile}} + P_{\text{parasite}} \\
 &= \frac{1.13 W^2}{2 A \rho (V^2 + v^2)^{1/2}} + \frac{C_{d,o} A}{8} \rho \sigma V_t^3 \left(1 + 3 \frac{V^2}{V_t^2}\right) + \frac{\rho}{2} V^3 f
 \end{aligned} \tag{A-1}$$

where the variables have been defined in Section 2.2. Let $V_o = \sqrt{\frac{W}{2 \rho A}}$, then Equation (A-1) reduces to dimensionless form

$$\frac{P}{W V_o} = \frac{1.13}{\left[\left(\frac{V}{V_o}\right)^2 + \left(\frac{v}{V_o}\right)^2\right]^{1/2}} + \frac{C_{d,o}}{16} \sigma \left(\frac{V_t}{V_o}\right)^3 \left(1 + 3 \frac{V^2}{V_t^2}\right) + \frac{1}{4} \frac{f}{A} \left(\frac{V}{V_o}\right)^3 \tag{A-2}$$

To find the speed $(V/V_o)_{\text{min}}$ at which the power required for flight is a minimum, P_{min} , we differentiate Equation (A-2) with respect to (V/V_o) and set the derivative equal to zero. A second differentiation has been performed and it was determined that the resultant velocity is indeed a minimum. The equation for the forward speed at minimum power then becomes:

$$\begin{aligned}
 \frac{d\left(\frac{P}{W V_o}\right)}{d\left(\frac{V}{V_o}\right)} = 0 &= \frac{-\frac{1.13}{2} \left(\frac{V}{V_o}\right)_{\text{min}} \left[1 + \frac{\left(\frac{V}{V_o}\right)_{\text{min}}^2}{\sqrt{4 + \left(\frac{V}{V_o}\right)_{\text{min}}^4}}\right]}{\left[\frac{1}{2} \left(\frac{V}{V_o}\right)_{\text{min}}^2 + \frac{1}{2} \sqrt{4 + \left(\frac{V}{V_o}\right)_{\text{min}}^4}\right]^{3/2}} \\
 &+ \frac{3}{8} C_{d,o} \sigma \left(\frac{V_t}{V_o}\right) \left(\frac{V}{V_o}\right)_{\text{min}} + \frac{3}{4} \frac{f}{A} \left(\frac{V}{V_o}\right)_{\text{min}}^2
 \end{aligned} \tag{A-3}$$

where the relationship between $\frac{v}{V_0}$ and $\frac{V}{V_0}$ is given by

$$\left(\frac{v}{V_0}\right)^2 = -\frac{1}{2} \left(\frac{V}{V_0}\right)^2 + \frac{1}{2} \sqrt{4 + \left(\frac{V}{V_0}\right)^4}$$

The roots of Equation (A-3) may be obtained by a graphical method. Let

$$F_1 \left[\left(\frac{V}{V_0}\right)_{\min} \right] = \frac{\frac{1.13}{2} \left(\frac{V}{V_0}\right)_{\min} \left[1 + \frac{\left(\frac{V}{V_0}\right)_{\min}^2}{\sqrt{4 + \left(\frac{V}{V_0}\right)_{\min}^4}} \right]}{\left[\frac{1}{2} \left(\frac{V}{V_0}\right)_{\min}^2 + \frac{1}{2} \sqrt{4 + \left(\frac{V}{V_0}\right)_{\min}^4} \right]^{3/2}}$$

and

$$F_2 \left[\left(\frac{V}{V_0}\right)_{\min} \right] = \frac{3}{8} C_{d,o} \sigma \left(\frac{V_t}{V_0}\right) \left(\frac{V}{V_0}\right)_{\min} + \frac{3}{4} \frac{f}{A} \left(\frac{V}{V_0}\right)_{\min}^2$$

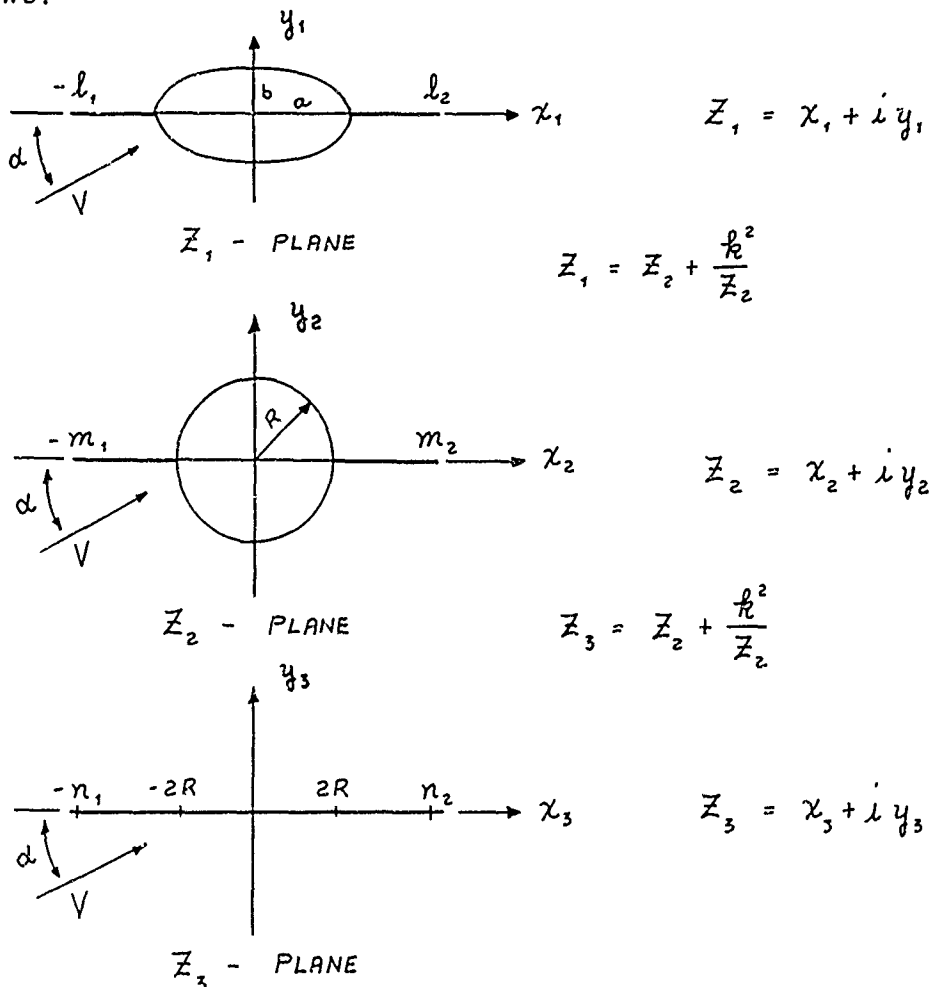
then the intersection of the curves of F_1 vs $\left(\frac{V}{V_0}\right)_{\min}$ and F_2 vs $\left(\frac{V}{V_0}\right)_{\min}$ will give the roots of Equation (A-3). In general, there are two real roots of Equation (A-3), but only the larger $\left(\frac{V}{V_0}\right)_{\min}$ is physically realistic. Figure 15 shows examples of typical roots found from the intersections of the curves of F_1 and F_2 with $C_{d,o} = 0.013$, $\frac{f}{A} = 0.010$ and $\sigma \frac{V_t}{V_0}$ varying between 0.8 to 3.6. Once $\left(\frac{V}{V_0}\right)_{\min}$ is obtained, Equation (A-2) may be used to calculate $\frac{P_{\min}}{WV_0}$.

APPENDIX B

Lift Coefficient for Finned Ellipse

The lift coefficient for a finned ellipse may be obtained by using conformal mapping. The flow over a finned ellipse in the physical plane is transformed to the equivalent flow over a flat plate in a transformed plane. The lift coefficient for a flat plate at an angle of attack is well known. The lift coefficient for the finned ellipse can then be computed through the appropriate transformations.

The transformations proceed through several conformal mappings as follows:



We first transform the finned ellipse to the finned circle through $Z_1 = Z_2 + \frac{k^2}{Z_2}$, with $k^2 = \frac{a^2 - b^2}{4}$. The points $-l_1$ and l_2 are transformed to $-m_1$ and m_2 respectively. The relationships between them are

$$l_1 = m_1 + \frac{k^2}{m_1}$$

and

$$l_2 = m_2 + \frac{k^2}{m_2}$$

The radius of the circle is $R = \frac{a+b}{2}$. Then, the finned circle is transformed to a flat plate by $Z_3 = Z_2 + \frac{R^2}{Z_2}$. The points $-n_1$ and n_2 are the corresponding points of $-m_1$ and m_2 .

Now we can calculate the lift for a flat plate. The lift coefficient for a flat plate at an angle of attack, α is given by

$$C_{L_3} = \frac{L_3}{\frac{1}{2} \rho V^2 d} = 2\pi\alpha$$

where

$$d = n_1 + n_2$$

To find the lift coefficient of the finned ellipse it is necessary to transform the chord of flat plate, d , back to the physical plane. Hence, we have

$$L_1 = L_3$$

$$C_{L_1} = \frac{L_1}{\frac{1}{2} \rho V^2 c} = C_{L_3} \frac{d}{c} = 2\pi\alpha \frac{d}{c} = 2\pi\alpha \left[\frac{n_1 + n_2}{l_1 + l_2} \right]$$

where n_1 and n_2 are related to l_1 and l_2 through

$$\begin{aligned} n_1 &= m_1 + \frac{R^2}{m_1} ; & m_1 &= \frac{1}{2} \left[l_1 + \sqrt{l_1^2 - (a^2 - b^2)} \right] \\ n_2 &= m_2 + \frac{R^2}{m_2} ; & m_2 &= \frac{1}{2} \left[l_2 + \sqrt{l_2^2 - (a^2 - b^2)} \right] \end{aligned}$$

APPENDIX C

Flapped Fuselage

Generally, the tail boom of the helicopter has either a circular or an elliptical shape. The concept of a mechanical flap may be applied to generate high lift. In Appendix B, the lift coefficient for an ellipse with fin has been calculated. Here we are going to illustrate the inverse procedure and use the same mapping technique to determine the shape of the mechanical flap. A flat plate with deflected straight flap is considered in the transformed plane and we wish to calculate the length and deflection angle of the corresponding straight flap in the physical plane.

Let the mapping from the \bar{z}_1 - plane to the \bar{z}_3 - plane be

$$\bar{z}_1 = \bar{z}_2 + \frac{k^2}{\bar{z}_2}$$

$$\bar{z}_3 = \bar{z}_2 + \frac{R^2}{\bar{z}_2}$$

or

$$\bar{z}_1 = \frac{\bar{z}_3 + \sqrt{\bar{z}_3^2 - 4R^2}}{2} + \frac{2k^2}{\bar{z}_3 + \sqrt{\bar{z}_3^2 - 4R^2}}$$

If this equation is split into real and imaginary parts, we obtain

$$x_1 = \left(1 + \frac{k^2}{R^2}\right) \frac{x_3}{2} + \frac{1}{2} \left(1 - \frac{k^2}{R^2}\right) \left[\frac{\sqrt{(x_3^2 - y_3^2 - 4R^2)^2 + 4x_3^2 y_3^2} + (x_3^2 - y_3^2 - 4R^2)}{2} \right]^{1/2}$$

$$y_1 = \left(1 + \frac{k^2}{R^2}\right) \frac{y_3}{2} + \frac{1}{2} \left(1 - \frac{k^2}{R^2}\right) \left[\frac{\sqrt{(x_3^2 - y_3^2 - 4R^2)^2 + 4x_3^2 y_3^2} - (x_3^2 - y_3^2 - 4R^2)}{2} \right]^{1/2}$$

where $\frac{a}{R}^2 = \frac{a^2 - b^2}{4}$ and $R^2 = \left(\frac{a+b}{2}\right)^2$. Hence, if x_3 and y_3 are given in the transformed plane, x_1 and y_1 can be calculated and plotted in the physical plane.

Two special cases have been carried out for illustration. Here a is chosen as a unit length, and all length scales are nondimensionalized by a . One case is for a flat plate of chord length $4R = 2.30$ (this corresponds to an ellipse in physical plane with $a = 1.0$, $b = 1.15$), flap length $N_2 = 1.0$ and deflection angle $\theta_3 = 60$ degrees. The flap length in the physical plane is $L_2 = 1.09$ and the deflection angle is $\theta_1 = 56$ degrees, approximately (Figure 16). Another case is a flat plate of chord length $4R = 4$ (this corresponds to a circle in the physical plane with $a = b = 1.0$), flap length $N_2 = 2.0$ and $\theta_3 = 60$ degrees. Then the flap length in the physical plane is $L_2 = 2.58$ and the deflection angle is $\theta_1 = 37$ degrees, approximately (Figure 17). Existing results for the lift of a flat plate with deflected flap (Reference 25) could be used to calculate the lift on the flapped fuselage cross-section.

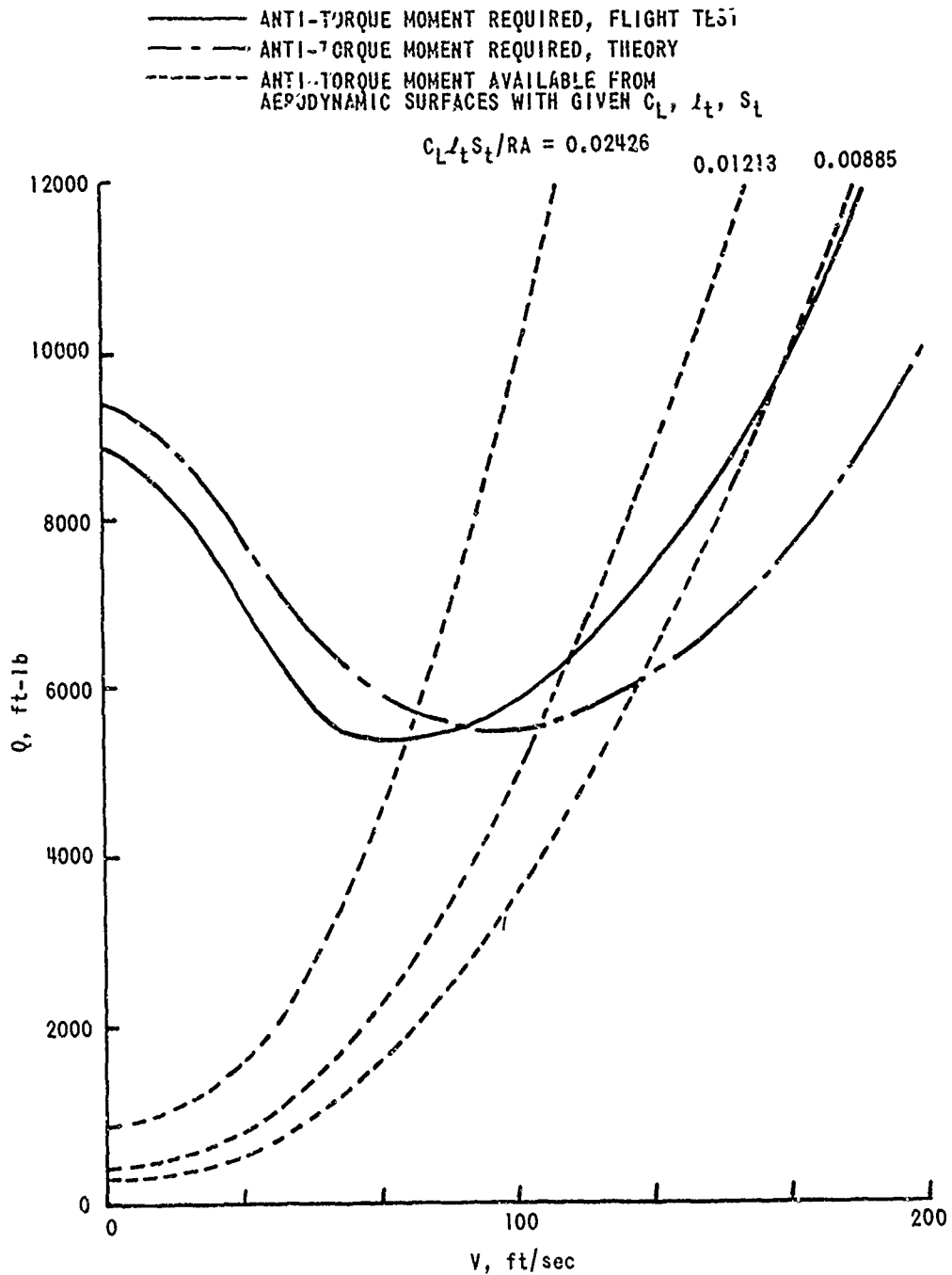


Figure 1 ANTI-TORQUE MOMENT AVAILABLE FROM AERODYNAMIC SURFACES TO BALANCE MAIN ROTOR TORQUE - BELL UH-1B HELICOPTER, 6550 LB GROSS WEIGHT, 314 RPM

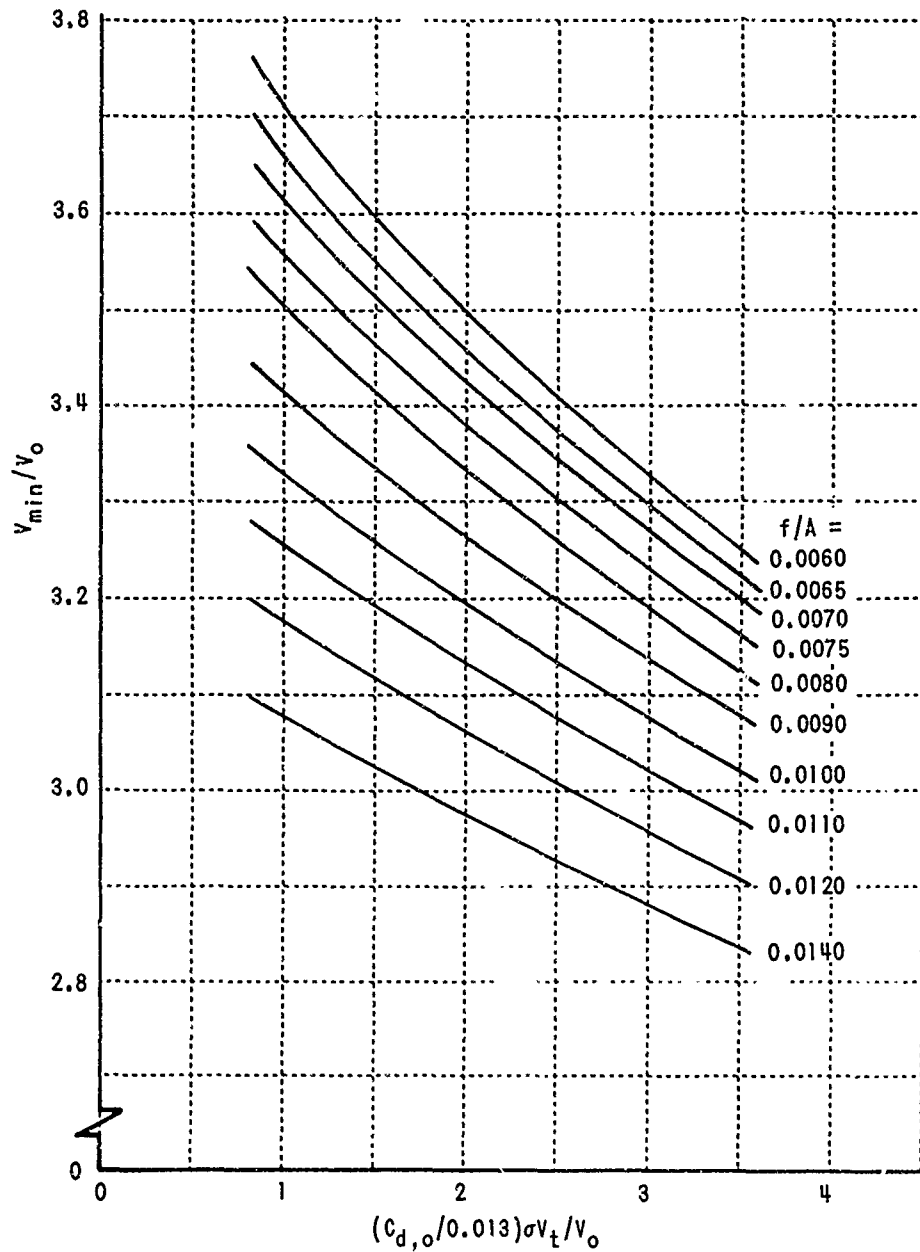


Figure 2 FLIGHT VELOCITY FOR MINIMUM POWER, V_{min} , AS A FUNCTION OF SECTIONAL DRAG COEFFICIENT, $C_{d,o}$, SOLIDITY, σ , TIP SPEED, V_t , AND EQUIVALENT FLAT PLATE AREA RATIO, f/A

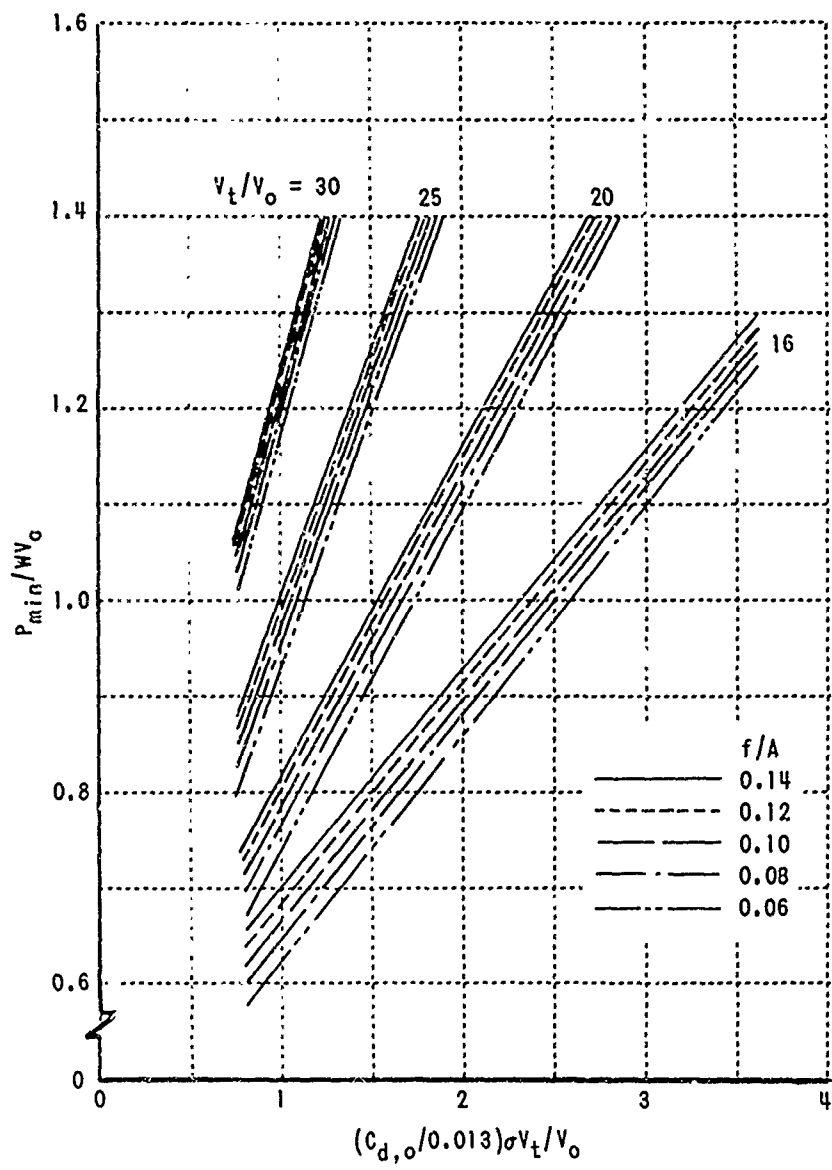


Figure 3 MINIMUM POWER, P_{min} , AS A FUNCTION OF SECTIONAL DRAG COEFFICIENT, $C_{d,o}$, SOLIDITY, σ , TIP SPEED, v_t , AND EQUIVALENT FLAT PLATE AREA, f/A

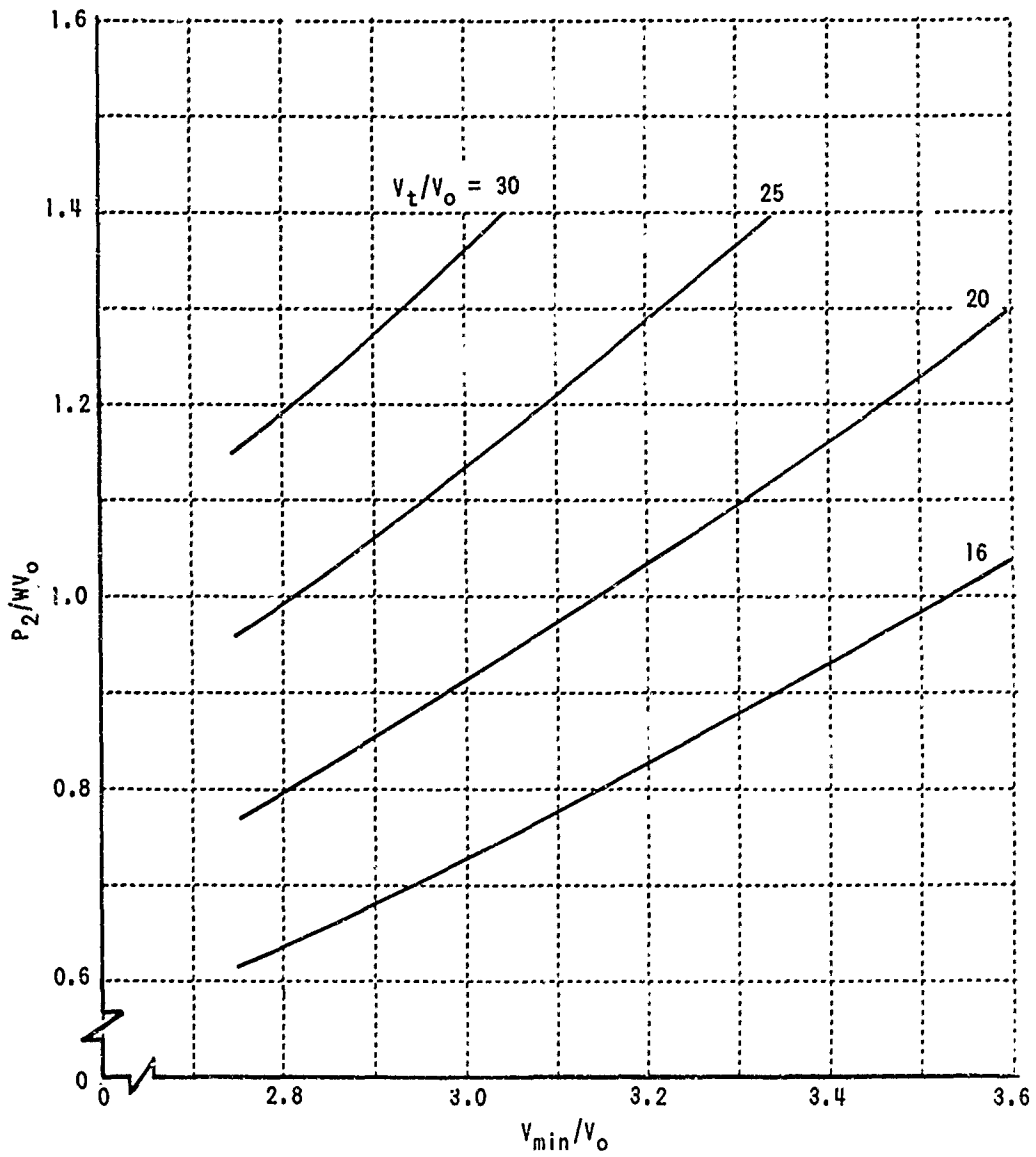


Figure 4 ANTI-TORQUE PERFORMANCE OF A 2% TAIL - POWER, P_2 , AS A FUNCTION OF FLIGHT VELOCITY FOR MINIMUM POWER, v_{min} , AND TIP SPEED, v_t

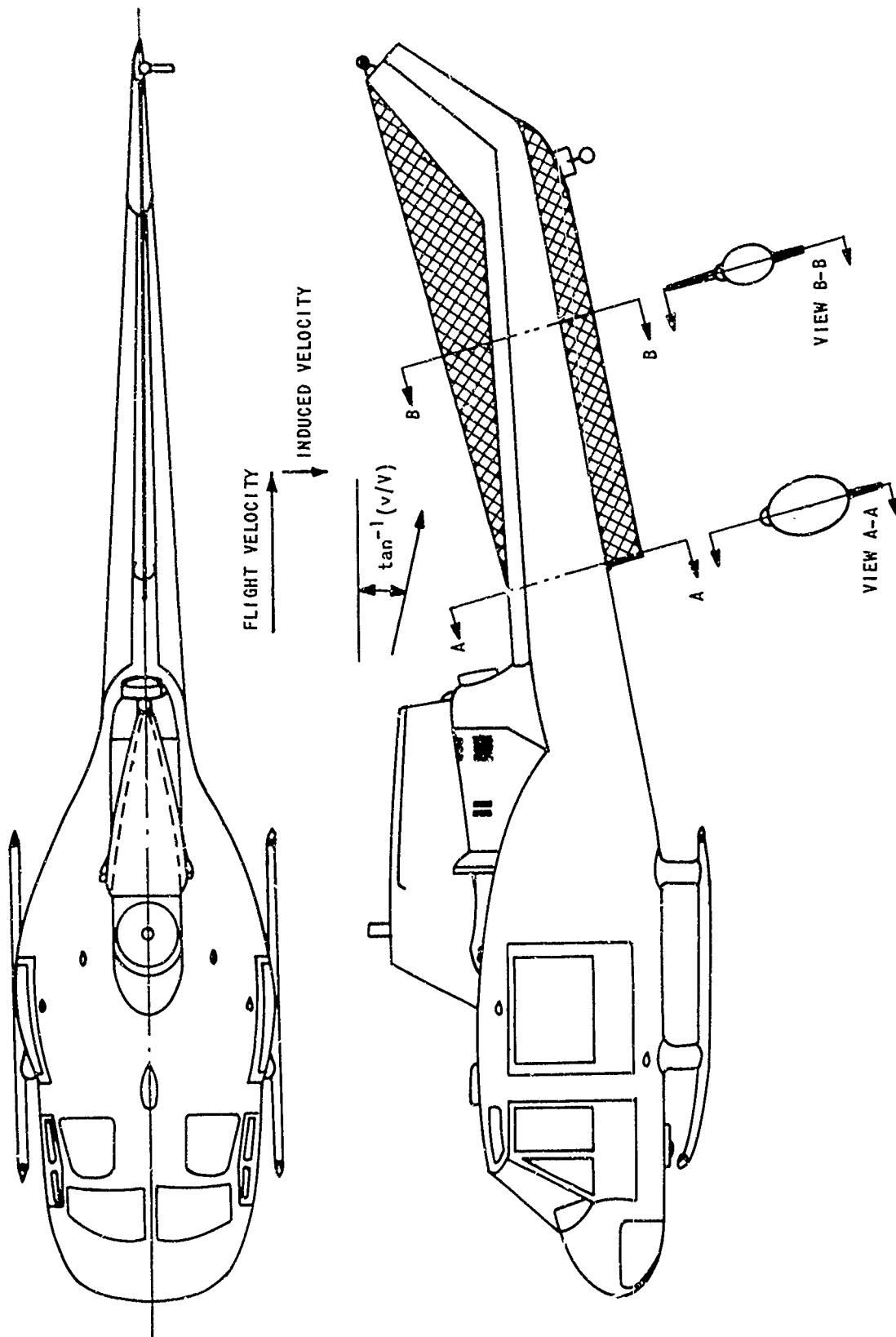
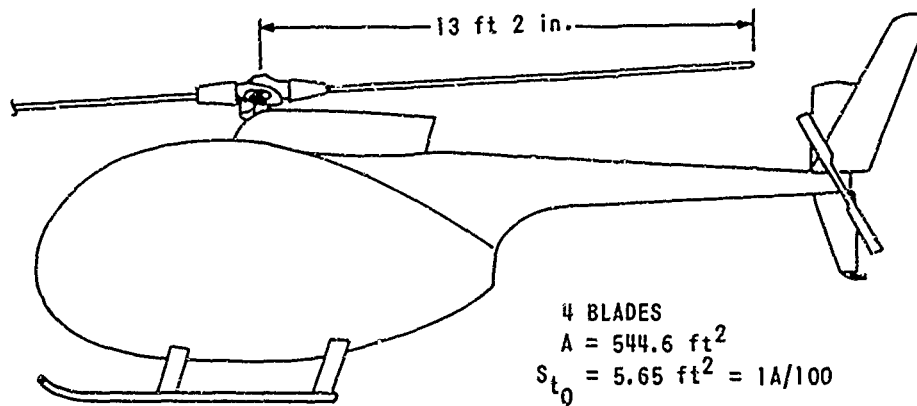
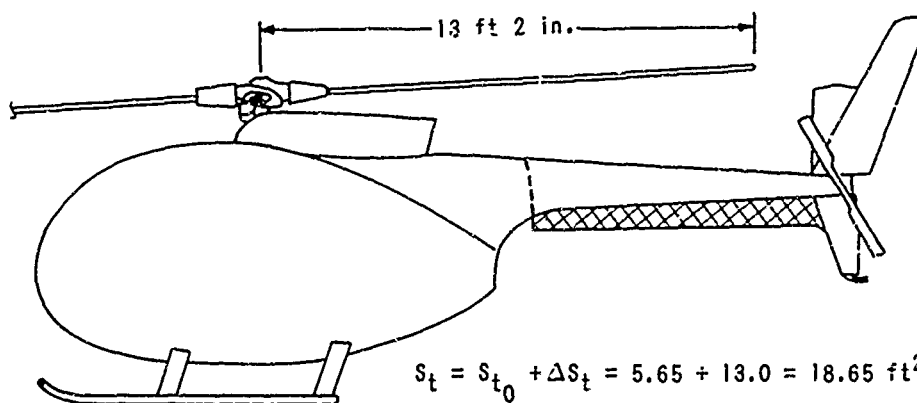


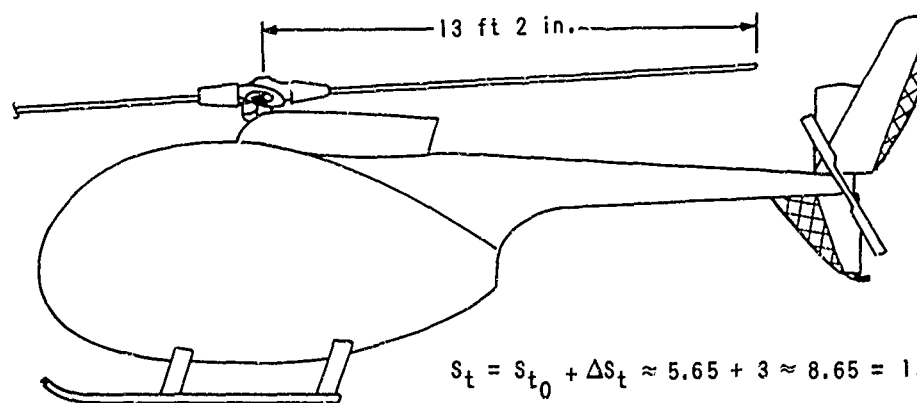
Figure 5. SCHEMATIC DIAGRAM OF A UH-1C WITH INCREASED TAIL AREA



a) ORIGINAL OH-6A HELICOPTER

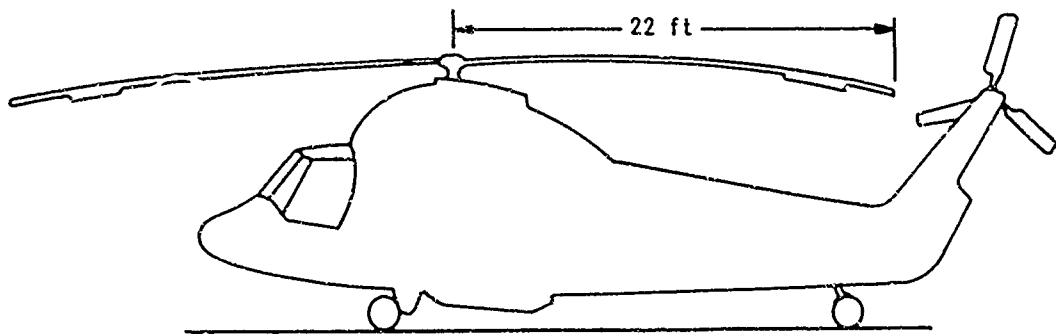


b) MODIFIED OH-6A WITH POSSIBLE SURFACES ADDED ON THE BODY



c) MODIFIED OH-6A WITH POSSIBLE SURFACES ADDED ON THE TAIL

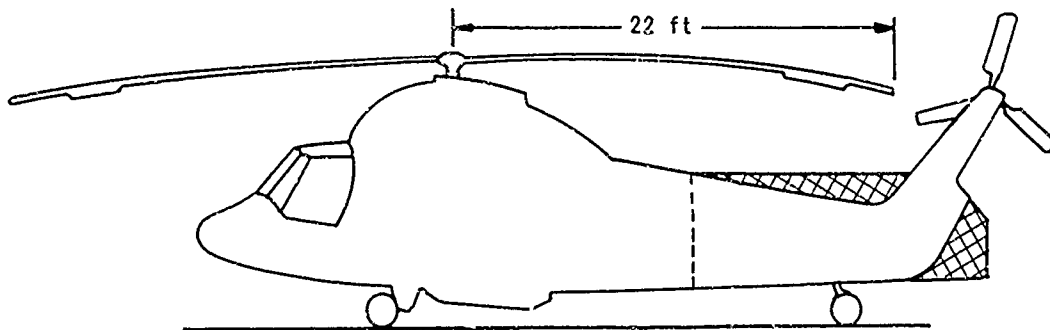
Figure 6. POSSIBLE OH-6A MODIFICATIONS



$$A = 1520,5 \text{ ft}^2$$

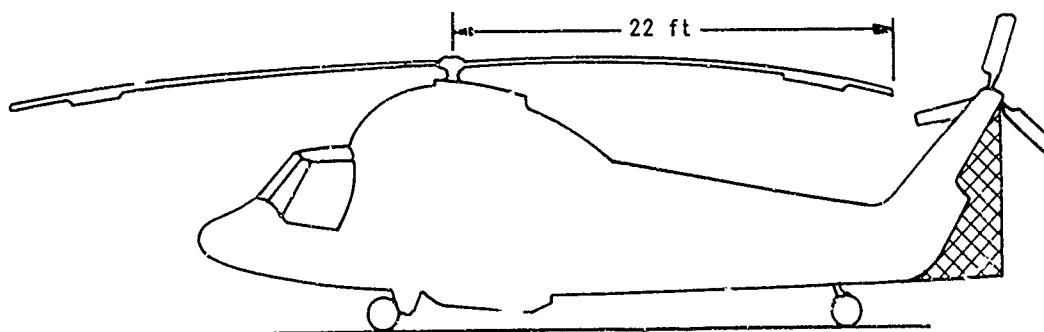
$$S_{t0} \approx 8 \text{ ft}^2 \approx 0.5A/100$$

a) ORIGINAL UH-2 HELICOPTER



$$S_t = S_{t0} + \Delta S_t \approx 8 + 70 \text{ ft}^2 \approx 78 \text{ ft}^2 \approx 5A/100$$

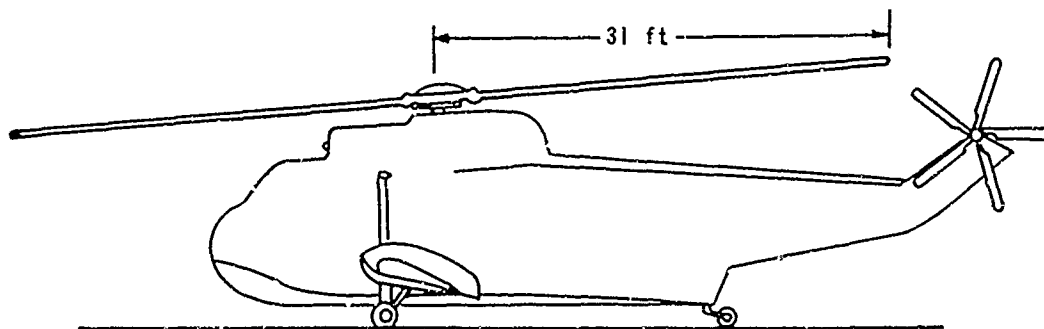
b) MODIFIED UH-2 WITH POSSIBLE SURFACES ADDED ON THE BODY



$$S_t = S_{t0} + \Delta S_t \approx 8 + 24 \text{ ft}^2 \approx 32 \text{ ft}^2 \approx 2.1A/100$$

c) MODIFIED UH-2 WITH POSSIBLE SURFACES ADDED ON THE TAIL

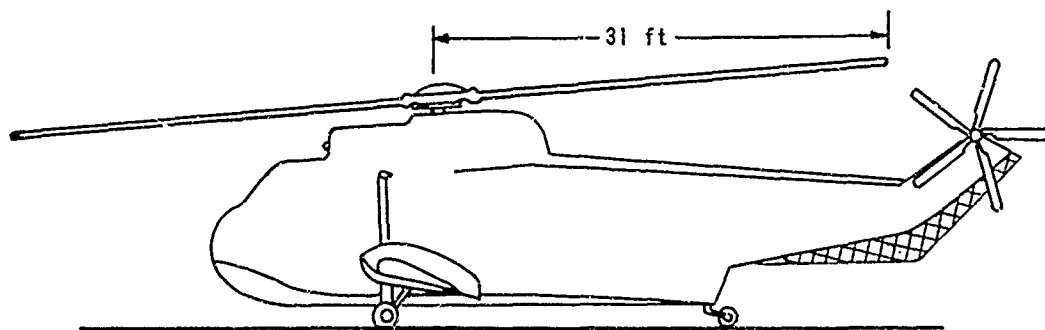
Figure 7. POSSIBLE UH-2 MODIFICATIONS



$$A = 3019 \text{ ft}^2$$

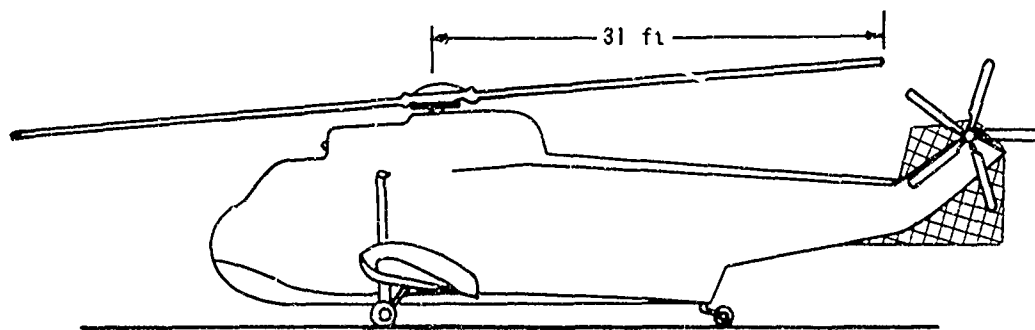
$$S_{t0} \approx 0$$

a) ORIGINAL SH-3D HELICOPTER



$$S_t = 74 \text{ ft}^2 \approx 2.4A/100$$

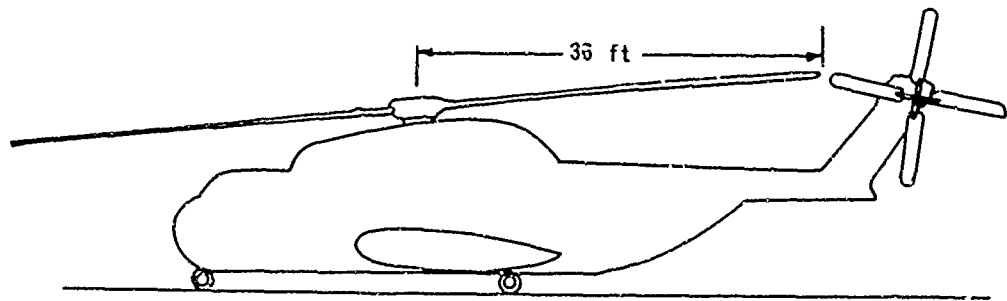
b) MODIFIED SH-3D WITH POSSIBLE SURFACES ON THE BODY



$$S_T \approx 52.5 \approx 1.7A/100$$

c) MODIFIED SH-3D WITH POSSIBLE SURFACES ADDED ON THE TAIL

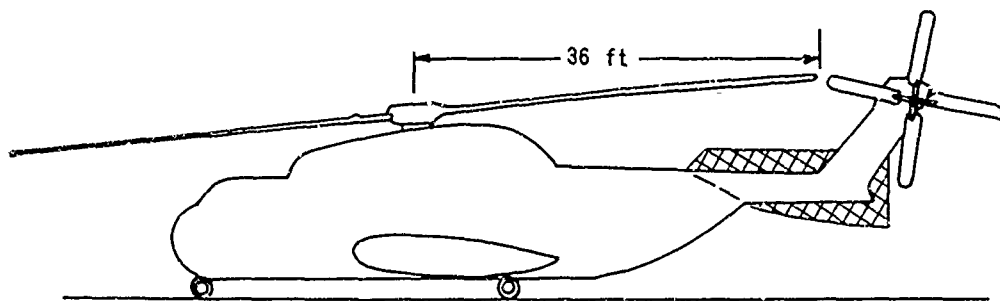
Figure 8. POSSIBLE SH-3D MODIFICATIONS



$$A = 4071.5$$

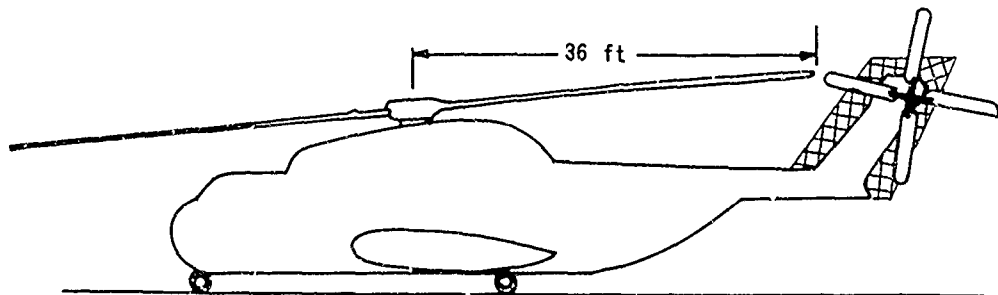
$$S_{t0} \approx 50 \text{ ft}^2 = 1.2A/100$$

a) ORIGINAL CH-53A HELICOPTER



$$S_t = S_{t0} + \Delta S_t \approx 50 + 60 \approx 110 \text{ ft}^2 \approx 2.7A/100$$

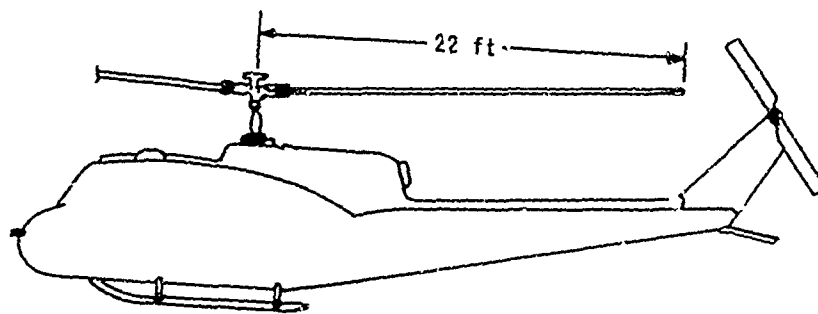
b) MODIFIED CH-53A WITH POSSIBLE SURFACES ADDED ON THE BODY



$$S_t \approx S_{t0} + \Delta S_t \approx 50 + 40 \approx 90 \text{ ft}^2 = 2.2A/100$$

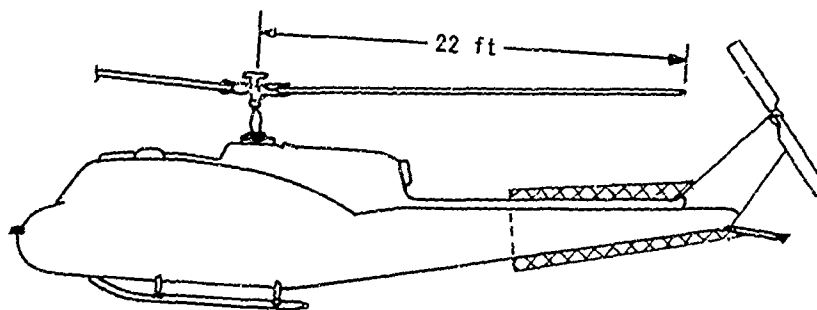
c) MODIFIED CH-53A WITH POSSIBLE SURFACES ADDED ON THE TAIL

Figure 9. POSSIBLE CH-53A MODIFICATIONS



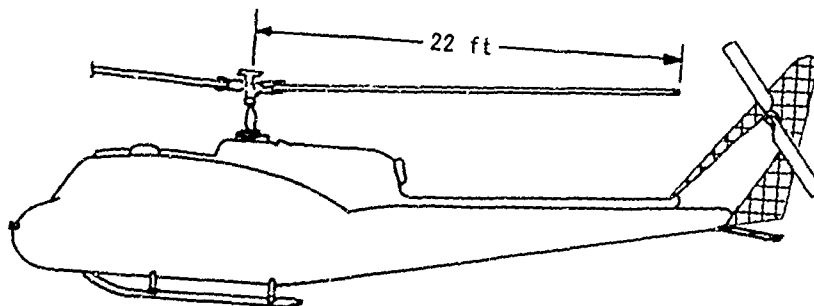
2 BLADES
 $A = 1520.5 \text{ ft}^2$
 $S_{t0} \approx 11 \text{ ft}^2 \approx 0.73A/100$

a) ORIGINAL UH-1C HELICOPTER



$$S_t = S_{t0} + \Delta S_t \approx 11 + 15 \approx 26 \text{ ft}^2 = 1.7A/100$$

b) MODIFIED UH-1C WITH POSSIBLE SURFACES ADDED ON THE BODY



$$S_t = S_{t0} + \Delta S_t \approx 11 + 15 \approx 26 \text{ ft}^2 = 1.7A/100$$

c) MODIFIED UH-1C WITH POSSIBLE SURFACES ADDED ON THE TAIL

Figure 10. POSSIBLE UH-1C MODIFICATIONS

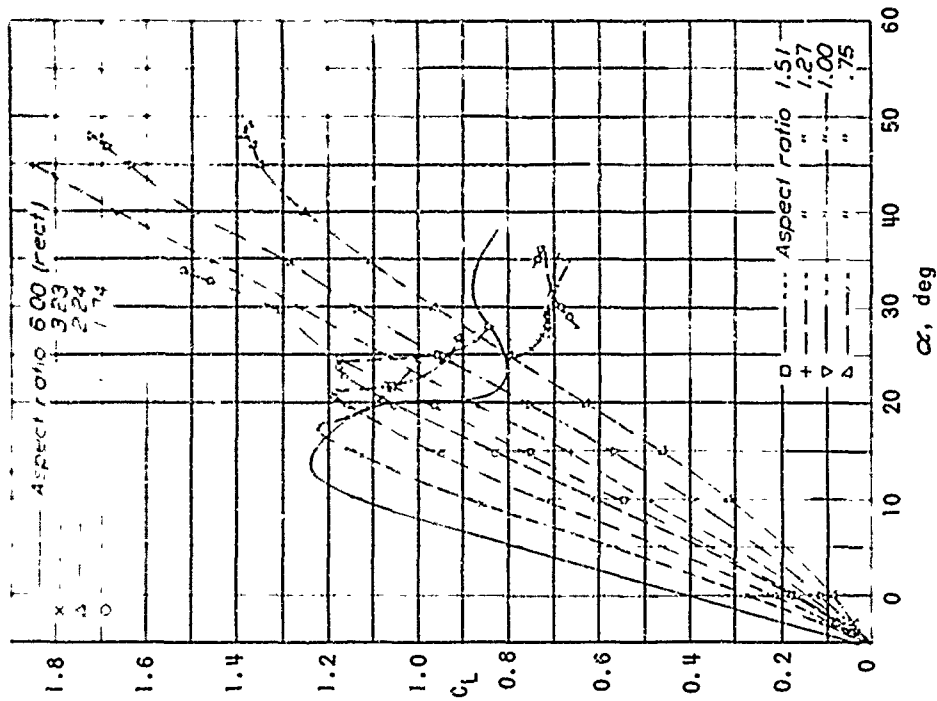


Figure 11b. EFFECTS OF ASPECT RATIO ON VARIATION OF LIFT COEFFICIENT WITH ANGLE OF ATTACK. SEMICIRCULAR TIPS. 0° YAW (DATA FROM REFERENCE 16)

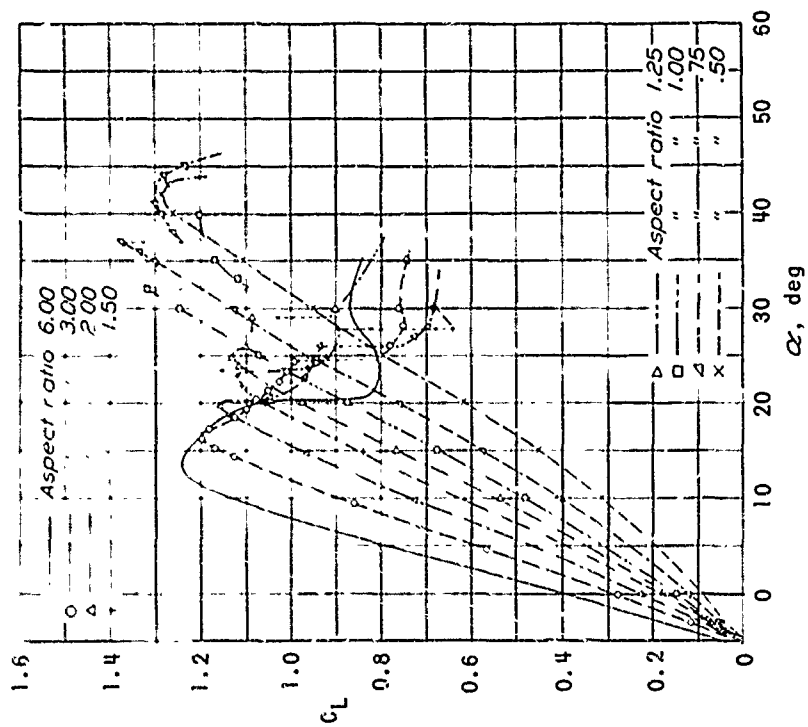


Figure 11a. EFFECTS OF ASPECT RATIO ON VARIATION OF LIFT COEFFICIENT WITH ANGLE OF ATTACK. RECTANGULAR TIPS. 0° YAW (DATA FROM REFERENCE 16)

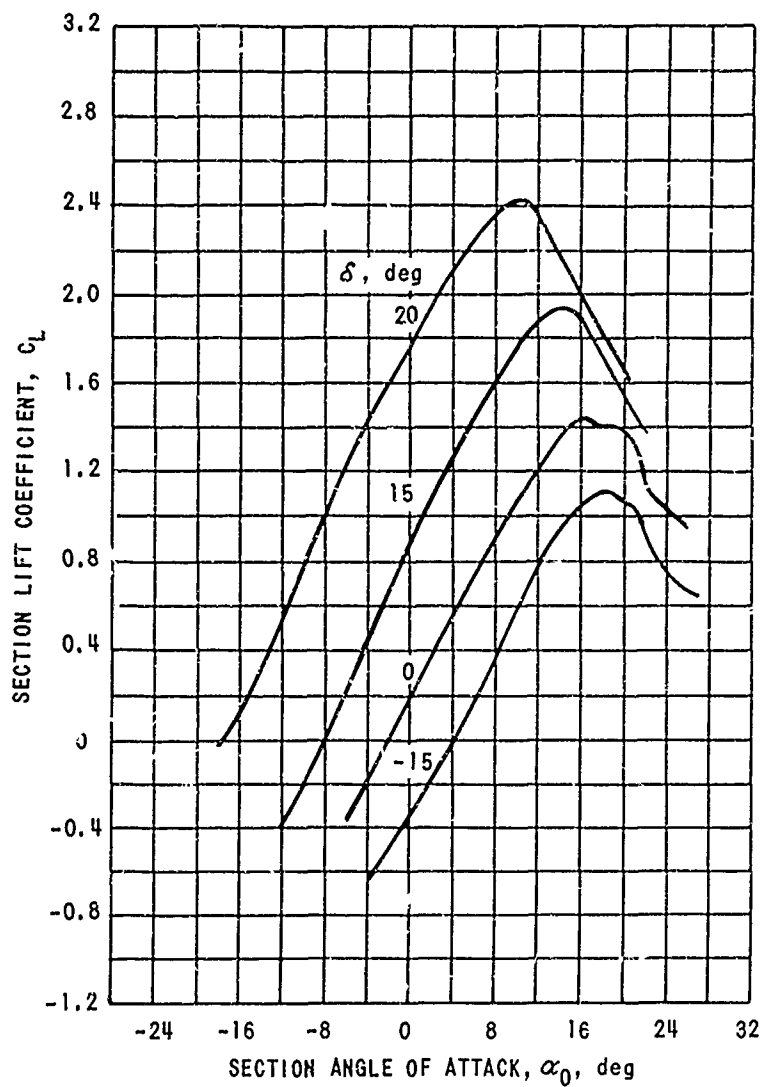


Figure 12. AERODYNAMIC CHARACTERISTICS OF THE NACA 66(215)-216 AIRFOIL SECTION WITH 0.20c SEALED PLAIN FLAP (REFERENCE 17)

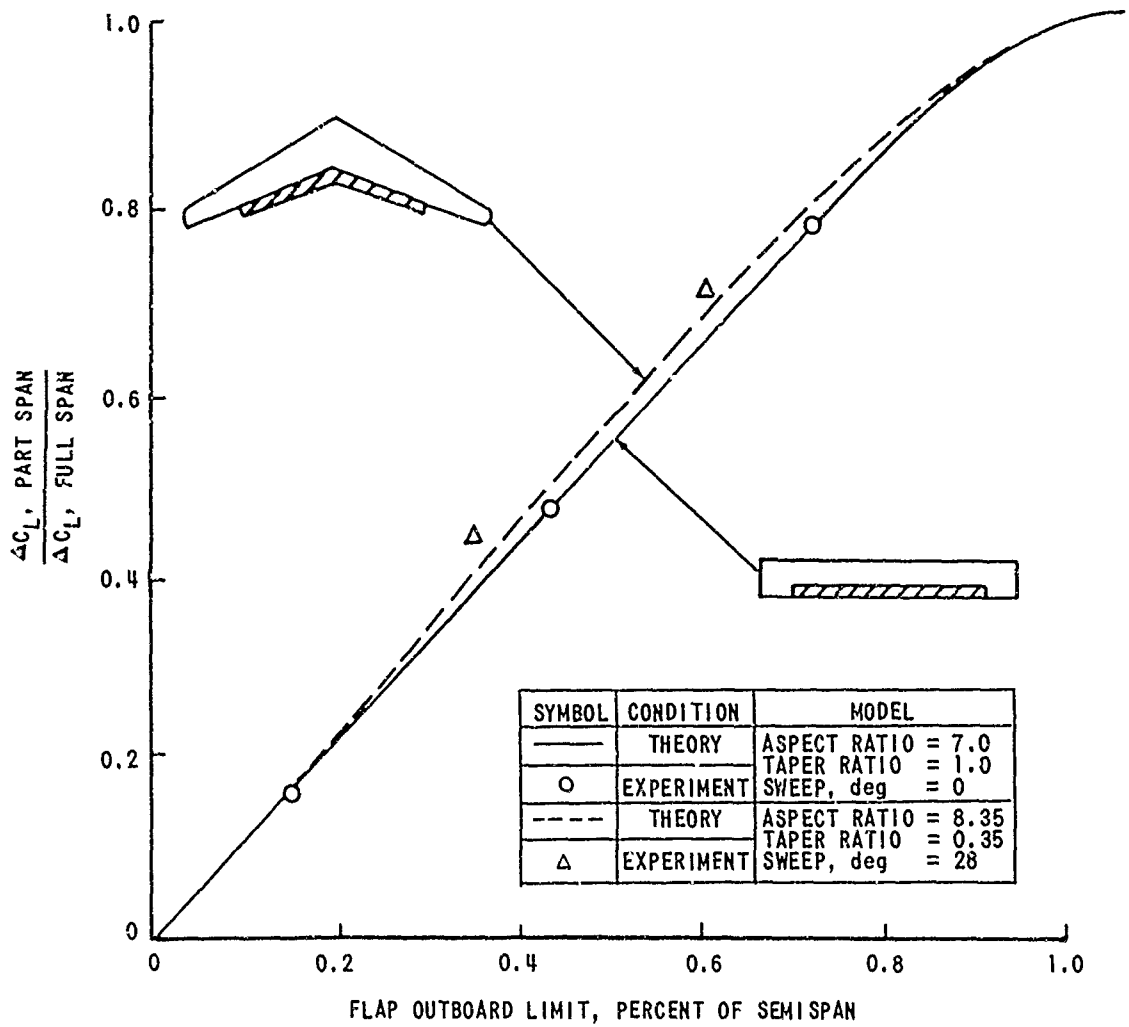


Figure 13. THEORETICAL AND EXPERIMENTAL PART-SPAN LIFT FACTORS FOR TWO MODELS (REFERENCE 18)

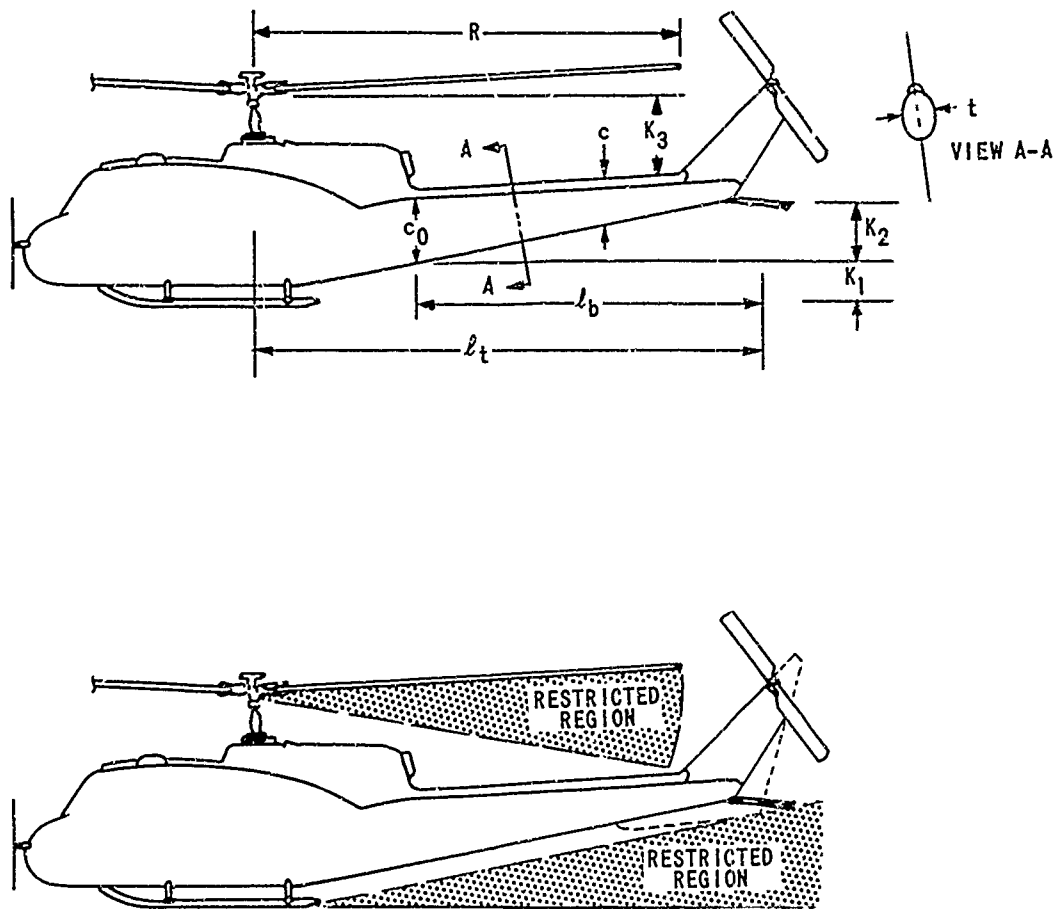


Figure 14. A SCHEMATIC DIAGRAM OF A UH-1A PROFILE WITH THE MORE IMPORTANT DIMENSIONS LABELED

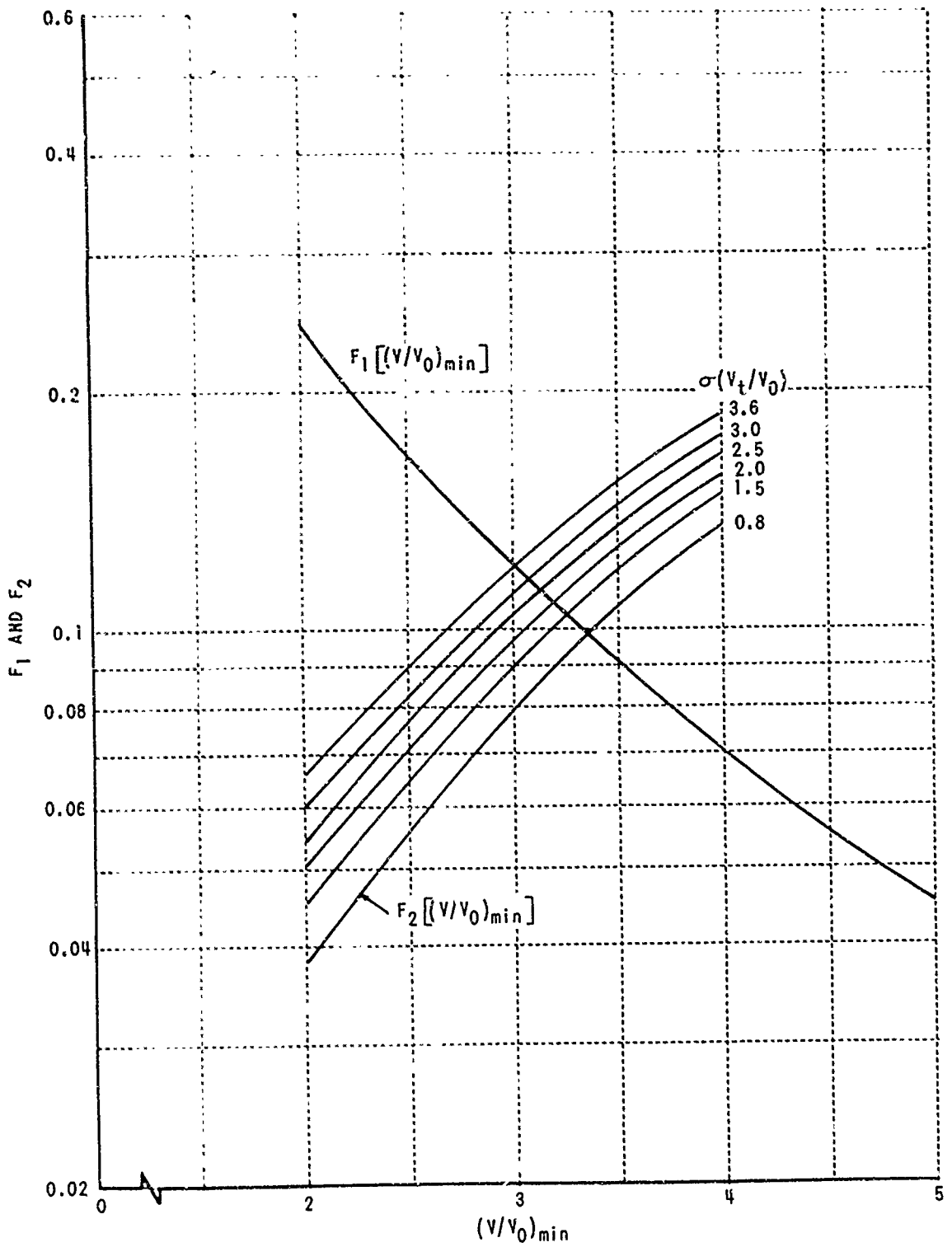


Figure 15. THE INTERSECTION OF THE CURVES OF F_1 AND F_2 WITH $C_{d,0} = 0.013$, $f/A = 0.01$, and $\sigma(V_t/V_0)$ VARYING BETWEEN 0.8 AND 3.6

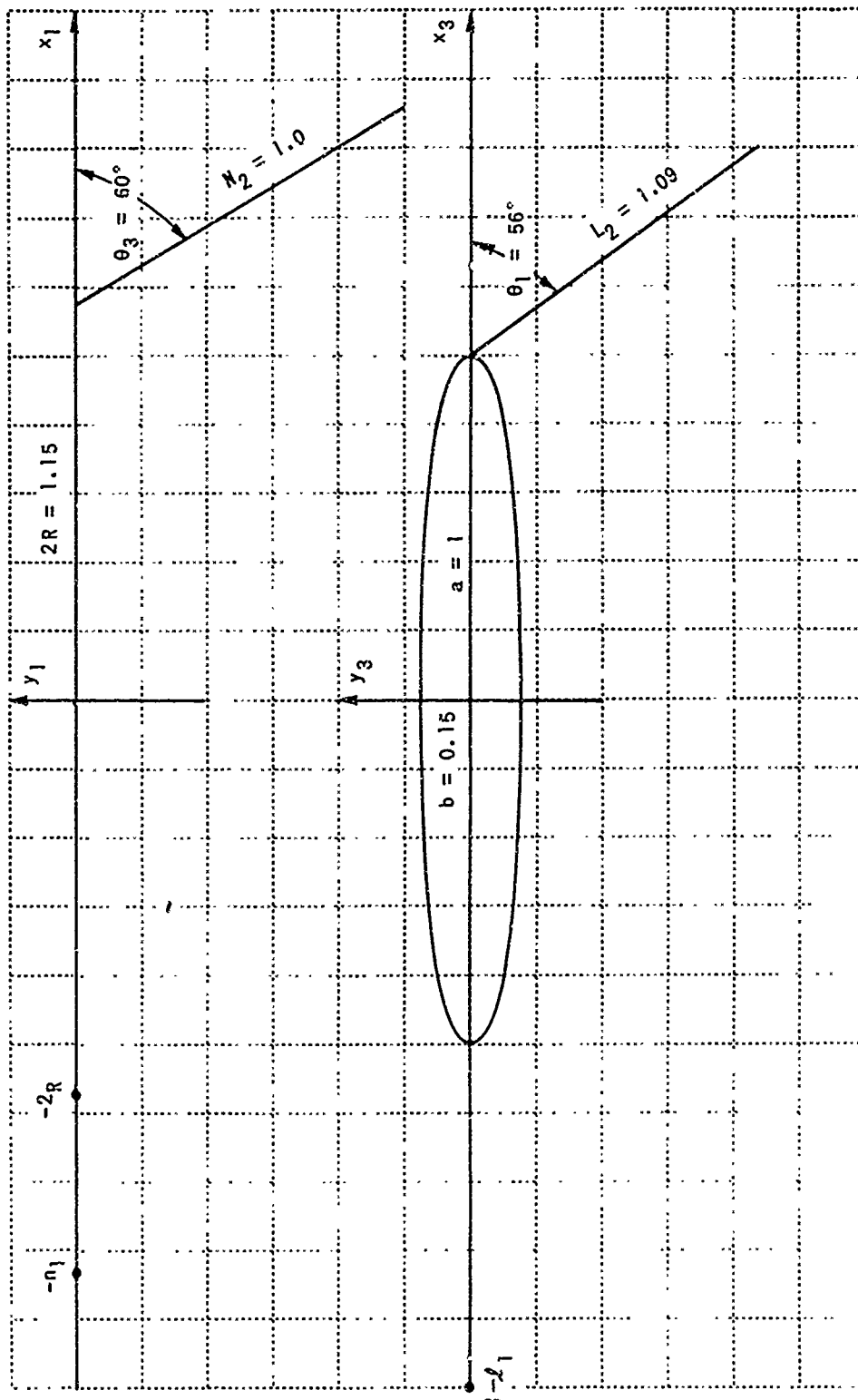


Figure 16. FLAPPED FUSELAGE OF ELLIPTICAL CROSS-SECTION
IN TRANSFORMED AND PHYSICAL PLANE

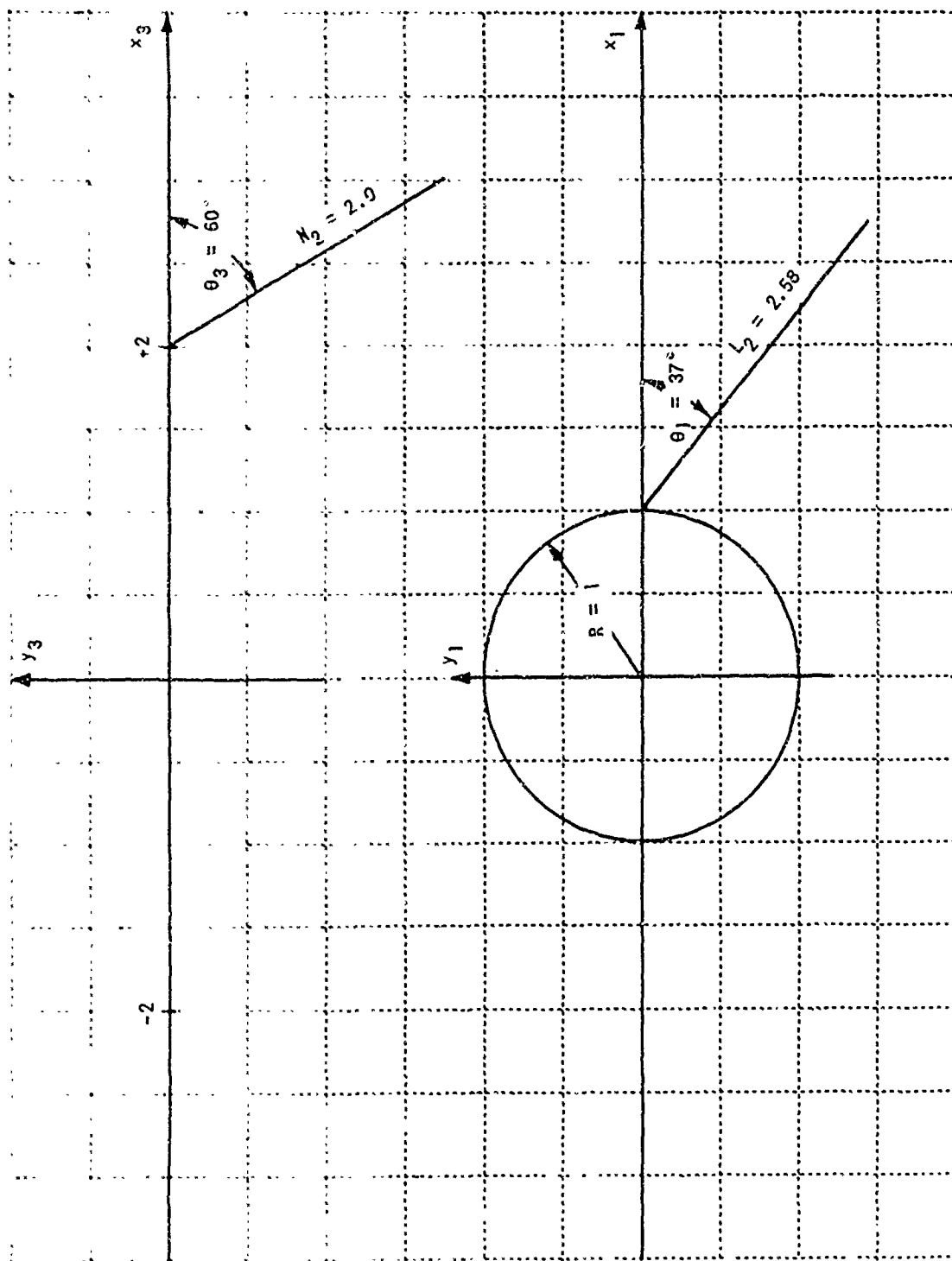


Figure 17. FLAPPED FUSELAGE OF CIRCULAR CROSS-SECTION IN TRANSFORMED AND PHYSICAL PLANE

Unclassified

Security Classification

DOCUMENT CONTROL DATA - R & D		
<i>(Security classification of title, body of abstract and indexing annotation must be entered when the overall report is classified)</i>		
1. ORIGINATING ACTIVITY (Corporate author) Cornell Aeronautical Laboratory, Inc. Buffalo, New York 14221		2a. REPORT SECURITY CLASSIFICATION Unclassified 2b. GRC(1/P)
3. REPORT TITLE THE FEASIBILITY AND USE OF ANTI-TORQUE SURFACES IMMERSSED IN HELICOPTER ROTOR DOWNWASH		
4. DESCRIPTIVE NOTES (Type of report and inclusive dates) Technical Report January 1968 - December 1969		
5. AUTHOR(S) (First name, middle initial, last name) Chee Tung, John C. Erickson, Jr., and Frank A. DuWaldt		
6. REPORT DATE February 1970	7a. TOTAL NO. OF PAGES	7b. NO. OF REFS
8a. CONTRACT OR GRANT NO. N00014-68-C-0241 b. PROJECT NO. NR 212-182 c. d.	9a. ORIGINATOR'S REPORT NUMBER(S) CAL No. BB-2584-S-2 9b. OTHER REPORT NO(S) (Any other numbers that may be assigned this report)	
10. DISTRIBUTION STATEMENT This document has been approved for public release and sale, its distribution is unlimited.		
11. SUPPLEMENTARY NOTES	12. SPONSORING MILITARY ACTIVITY Office of Naval Research Aeronautics, Code 461 Arlington, Virginia 22217	
13. ABSTRACT An analytical investigation was made of the effectiveness of anti-torque aerodynamic surfaces immersed in helicopter rotor downwash. It is shown that additional vertical tail surface having areas equal to about two percent of the main rotor disk area could provide torque trim for speeds above about 75 ft/sec for representative current vehicles.		

DD FORM 1473
1 NOV 65

REPLACES DD FORM 1473, 1 JAN 64, WHICH IS
OBSOLETE FOR ARMY USE.

Unclassified

Security Classification

Unclassified

Security Classification

14. KEY WORDS	LINK A		LINK B		LINK C	
	ROLE	WT	ROLE	WT	ROLE	WT
Helicopter Tail Rotor Anti-Torque Devices						

Unclassified

Security Classification